

AN ACTIVE POWER SUPPLY FILTER WITH ULTRA WIDE BANDWIDTH

A Thesis
Submitted to the Graduate Faculty
of the
North Dakota State University
of Agriculture and Applied Science

By
Brian James Booth

In Partial Fulfillment of the Requirements
for the Degree of
MASTER OF SCIENCE

Major Department:
Electrical and Computer Engineering

May 2016

Fargo, North Dakota

NORTH DAKOTA STATE UNIVERSITY

Graduate School

Title

AN ACTIVE POWER SUPPLY FILTER WITH ULTRA WIDE BANDWIDTH

By

Brian James Booth

The supervisory committee certifies that this thesis complies with North Dakota State University's regulations and meets the accepted standards for the degree of

MASTER OF SCIENCE

SUPERVISORY COMMITTEE:

Dr. Benjamin D. Braaten

Chair

Dr. Ivan T. Lima, Jr.

Dr. Debasis Dawn

Dr. Davis Cope

Approved:

July 6th, 2016

Date

Dr. Scott Smith

Department Chair

ABSTRACT

An active transformerless common mode filter is designed for use with switching mode power supplies with a switching frequency greater than 1MHz. The filter utilizes an amplifier in a voltage sensing current adjusting architecture to cancel out common mode noise generated by the switching power supply. The filter is analyzed using a transfer function, simulation, and measurements. Several possible feedback configurations are examined and benefits of different configurations are explained. The active filter is shown to have superior performance to only passive components at frequencies up to 20MHz. Spectral domain, time domain, and S21 measurements are given to show the filter's effectiveness.

ACKNOWLEDGEMENTS

I would like to thank my advisor, Dr. Braaten, for his support and patience as I worked to complete my thesis. His guidance and suggestions were always appreciated.

I would like to thank my committee Dr. Davis Cope, Dr. Debasis Dawn, and Dr. Ivan Lima. They have all taught me many things in their courses. I appreciate their support and suggestions on my thesis work.

I would like to thank John Deere for sponsoring my Master's Degree. Specifically I would like to thank my coworkers for their encouragement and reminders to get my thesis work done.

I would like to thank my wife Kimi for helping me complete my thesis, even when it seemed like it would never get done. She truly has been my encouraging advocate throughout this whole process.

DEDICATION

To my wonderful wife Kimi and my daughter Rozalyn.

TABLE OF CONTENTS

ABSTRACT	iii
ACKNOWLEDGEMENTS	iv
DEDICATION	v
LIST OF FIGURES	viii
CHAPTER 1. INTRODUCTION	1
CHAPTER 2. THEORY AND DESIGN	2
2.1. Introduction	2
2.2. Conducted and Radiated Emissions	2
2.3. Switched-Mode Power Supplies	4
2.3.1. Switched-Mode Power Supplies as a source of EMI	4
2.3.2. Equivalent Common Mode Noise Source Model	6
2.4. Filtering	8
2.4.1. Definition of S21	8
2.4.2. Traditional Filtering	9
2.4.3. Active Filtering	9
2.4.4. Voltage Sensing Current Adjusting Architecture	12
CHAPTER 3. RESULTS	14
3.1. Introduction	14
3.2. Analysis of Proposed Active Filter	14
3.2.1. Transfer Function	14
3.2.2. Determination of Z_{feedback}	14
3.2.3. Ideal Simulation	17
3.2.4. Bandwidth Limited Simulation	17
3.3. Filter Synthesis	19

3.4. Measurements	25
3.4.1. S21 Measurment	25
3.4.2. Frequency Domain	33
3.4.3. Time Domain	37
CHAPTER 4. CONCLUSION	40
BIBLIOGRAPHY	41
APPENDIX	43

LIST OF FIGURES

<u>Figure</u>	<u>Page</u>
2.1. LISN as defined in CISPR 25	3
2.2. Radiated Emissions Test Setup	3
2.3. CISPR 25 LISN Impedance from port B to P	4
2.4. DC to DC Buck Switched-Mode Power Supply	5
2.5. Switch Node Voltage for Switched-Mode Power Supply	5
2.6. Heat Sink Cross Section	6
2.7. DC to DC Buck Switched-Mode Power Supply with Parasitic Heat Sink Capacitance	7
2.8. CISPR 25 Setup with DC to DC Buck Switched-Mode Power Supply	7
2.9. CISPR 25 Setup with an Equivalent Common Mode Noise Source Model	8
2.10. Traditional Power Supply Filter	9
2.11. Current Sensing Current Adjusting Schematic	10
2.12. Voltage Sensing Current Adjusting Schematic	10
2.13. Current Sensing Voltage Adjusting Schematic	11
2.14. Voltage Sensing Voltage Adjusting Schematic	11
2.15. Proposed Voltage Sensing Voltage Adjusting Schematic	12
2.16. VSCA Filter in System Application	13
3.1. System schematic with proposed VSCA filter for analysis	15
3.2. MATLAB plot of voltage across the LISN impedance predicted by 3.1 using three possible feedback configurations, a shorted feedback network, a 100Ω feedback network, and a 1GΩ feedback network.	15
3.3. MATLAB plot comparing four 1nF capacitors connected in parallel with Z_{LISN} to proposed filter with shorted feedback.	16
3.4. Plot of S21 comparing MATLAB code using 3.1 to Keysight ADS simulation using ideal an op-amp and a shorted feedback network.	17
3.5. Plot of S21 comparing MATLAB code using 3.1 to Keysight ADS simulation using ideal an op-amp and a 100Ω feedback network.	18

3.6. Plot of S21 comparing MATLAB code using 3.1 with 1G Ω feedback network to Keysight ADS simulation using an ideal op-amp with a gain of 10000 and an open feedback network.	19
3.7. Bandwidth limited simulation circuit schematic in Keysight's ADS 2015.	20
3.8. S21 Bandwidth limited circuit simulation results using three different feedback network configurations: a shorted feedback network, a 100 Ω network, and an open feedback network. The op amp was set to have a bandwidth of 400MHz.	20
3.9. Results of S21 bandwidth limited circuit simulation with 100 Ω feedback compared to MATLAB predicted results using 3.1 with a 100 Ω feedback configuration.	21
3.10. Voltage magnitude at output of op amp for both an ideal and bandwidth limited circuit simulation with 100 Ω .	22
3.11. Voltage phase at output of op amp for both an ideal and bandwidth limited circuit simulation with 100 Ω .	23
3.12. Circuit simulation with 100 Ω feedback and a bandwidth limited op-amp with three different bandwidths, 100MHz, 200MHz, and 400MHz.	24
3.13. Photo of designed circuit. A quarter is given for size comparison.	25
3.14. Schematic of synthesized circuit, TI's THS4271 was used for U1.	26
3.15. Test Setup for S21 Measurements	27
3.16. Plot of S21 with a 10dBm source applied to circuits under test with a 50 Ω resistor in series with a 220pF capacitor as source impedance. The test circuit uses three different possible feedback networks, a shorted network, an open network, and an open circuit network. The plot compares the active filter to four 1nF capacitors and a setup with no filter present.	28
3.17. Plot of measured S21 of test circuit with an open feedback configuration compared to MATLAB code using 3.1 with a 1G Ω feedback network.	29
3.18. Plot of measured S21 of test circuit with a 100 Ω feedback configuration compared to MATLAB code using 3.1 with a 100 Ω feedback network.	30
3.19. Plot of measured S21 of test circuit with a 100 Ω feedback configuration compared to measured S21 of circuit using four 1nF capacitors connected in parallel.	31
3.20. Plot of measured S21 of test circuit with a shorted feedback configuration compared to MATLAB code using 3.1 with a shorted feedback network.	32
3.21. Plot of measured S21 of test circuit with a shorted feedback configuration compared to measured S21 of circuit using four 1nF capacitors connected in parallel.	33
3.22. Plot of measured S21 of test circuit with a shorted feedback configuration compared to measured S21 of test circuit using a 100 Ω feedback configuration.	34

3.23. Test setup for time and frequency measurements.	35
3.24. Plot of spectral measurements with a 1MHz square wave applied to circuits under test with a 50Ω resistor in series with a 220pF capacitor as source impedance. The input waveform was 3V peak to peak. The proposed filter circuit was tested with a shorted feedback configuration, 100Ω feedback configuration, and open feedback configuration. The proposed filter measurements are also compared to four 1nF capacitors in parallel and a test setup without a filter.	36
3.25. Plot of spectral measurements using the same setup as Figure 3.24, except with a larger frequency band shown.	37
3.26. Time domain plot of input to the test circuit compared to the output of the test circuit using a shorted feedback configuration, a 100Ω feedback configuration, and an open feedback configuration. For reference, an output with no filter circuit is also shown. . .	38
3.27. Zoomed in time domain plot of filter output with a shorted feedback configuration, a 100Ω feedback configuration, and an open feedback configuration. For reference, the input waveform and an output with no filter circuit is also shown.	38

CHAPTER 1. INTRODUCTION

Recently, switched mode power supplies (SMPS) in the 1-10 MHz frequency range have become commercially available. The work in [1] has shown a SMPS capable of delivering 25W while operating with a switching frequency of 27MHz. The increased power rating with the higher frequency of new switching power supplies creates new challenges in electromagnetic compatibility. Electromagnetic compatibility is the study of how devices interact with other devices and themselves through an electromagnetic perspective. The field is concentrated around trying to meet a balance between designing that meets cost and performance goals and designing to meet regulations for the amount of electromagnetic interference a product is allowed to emit or must be able to absorb.

This thesis is concentrated on the topic of filtering switched mode power supplies and the interference created by them. The problem of interference created by switched mode power supplies is well studied and understood [2]. A newer perspective for dealing with interference from switching mode power supplies is to use an active filter. Active filters allow for filtering in frequency ranges that were previously much more difficult to filter for traditional power supply filter components, due to the large size common mode choke required for high power applications.

The rest of this thesis is organized as follows. Chapter 2 presents product conducted and radiated emissions problems and develops a common mode noise source model for switched mode power supplies. Several active filtering topologies are presented. The voltage sensing current adjusting architecture is investigated in more detail. Chapter 3 expands on the voltage sensing current adjusting architecture even further. A transfer function is derived and results of simulations are shown. Several possible feedback configurations are presented and discussed. The proposed filter is then synthesized and spectral domain, time domain, and S21 measurements are presented. Chapter 4 concludes the thesis.

CHAPTER 2. THEORY AND DESIGN

2.1. Introduction

This chapter presents the problem of conducted and radiated emissions of a system. A typical switching-mode power supply is shown and a noise source model is given. A simplified noise source model for the switching-mode power supply is derived and finally different filtering solutions, including active filtering, are presented to help pass a conducted or radiated emissions test.

2.2. Conducted and Radiated Emissions

One of the core principles of Electromagnetic Compatibility (EMC) is measuring the disturbances a device or system creates. These disturbances are measured in two different ways. Conducted emissions are voltage and/or current measurements taken directly from the power supply, control, and/or signal lines of a device under test (DUT). Conducted emissions are measured either using a special port on a Line Impedance Stabilizing Network (LISN) or by using a current probe. Radiated emissions are disturbances caused by capacitive coupling, inductive coupling, or full wave radiation from a DUT. Radiated emissions are measured using an antenna [3].

A conducted or radiated emissions test will feed power to a DUT through a set of LISNs. A LISN is a 3 port device that serves two purposes in a conducted or radiated emissions test [3]. The first purpose is to provide a known stable impedance for the power input to the DUT so test results are repeatable from one test to the next. The second purpose is to provide a method to measure conducted emissions from the power supply lines of a DUT. The schematic for a LISN as defined by the international standard CISPR 25 is given in Figure 2.1. A simple schematic for the connection of a DUT during a conducted emissions test is given in Figure 2.2 [4]. The impedance between the ports B and P of the LISN are given in Figure 2.3.

From Figure 2.3 LISNs generally have an impedance of 50Ω between ports B and P. The 50Ω port on the LISNs is used for measuring the conducted emissions of a DUT. To guarantee that a device will pass a conducted emissions test a designer simply needs to make sure that the DUT limits the amount of current that flows through the 50Ω measuring port. In systems with a noise source modeled as a high impedance current source, a designer simply needs to place a large enough capacitance on the power supply inputs to bypass the LISN measuring port [3].

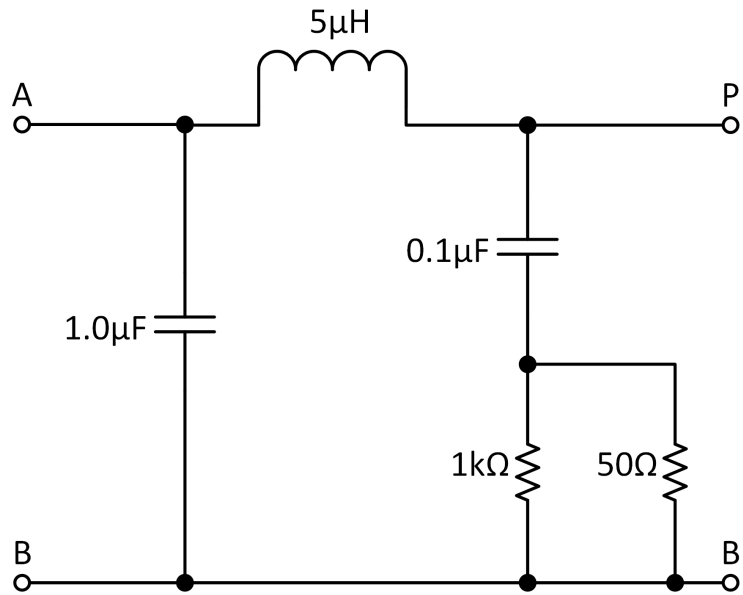


Figure 2.1. LISN as defined in CISPR 25

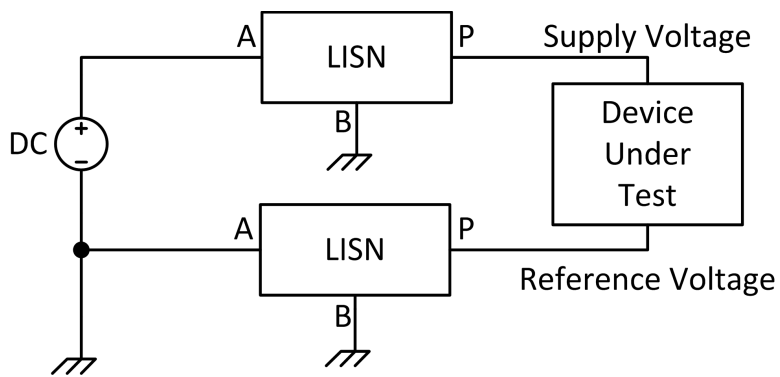


Figure 2.2. Radiated Emissions Test Setup

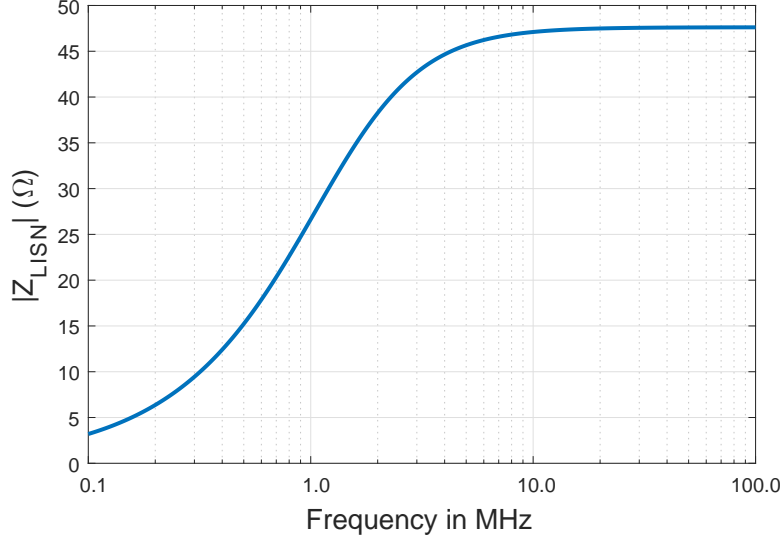


Figure 2.3. CISPR 25 LISN Impedance from port B to P

2.3. Switched-Mode Power Supplies

SMPSs are popular types of power supplies that are known for their efficiency and relatively small size. An example schematic for a DC to DC buck SMPS is given in Figure 2.4. The main advantage of a SMPS is derived from SW_1 and SW_2 . When SW_1 closed, SW_2 is open and V_N is the same voltage as the input voltage to the supply. When SW_1 is open, SW_2 is closed and V_N is pulled to the supply reference voltage. The frequency of the closing and opening of SW_1 determines the inductance of the inductor L_{SW} . The higher the frequency, the less inductance required. When SW_1 is non-ideal, the higher switching frequency creates more losses due to a larger amount of time spent switching SW_1 on and off [5], [2].

2.3.1. Switched-Mode Power Supplies as a source of EMI

The increased efficiency and relatively small size of an SMPS comes with a trade-off of increased electromagnetic interference (EMI). As stated earlier, from Figure 2.4 the voltage at the node V_N is switching between the input supply voltage and the reference voltage at the switching frequency of the SMPS. The voltage looks like the waveform given in Figure 2.5 [6].

Additionally, due to the power dissipation in SW_1 from both conduction and switching losses, SW_1 is often thermally connected to, but electrically isolated from, a heat sink that may be connected to some sort of system chassis or earth ground. A diagram of the heat sink interface is given in Figure 2.6. A close examination of the heat sink reveals that a capacitance exists between

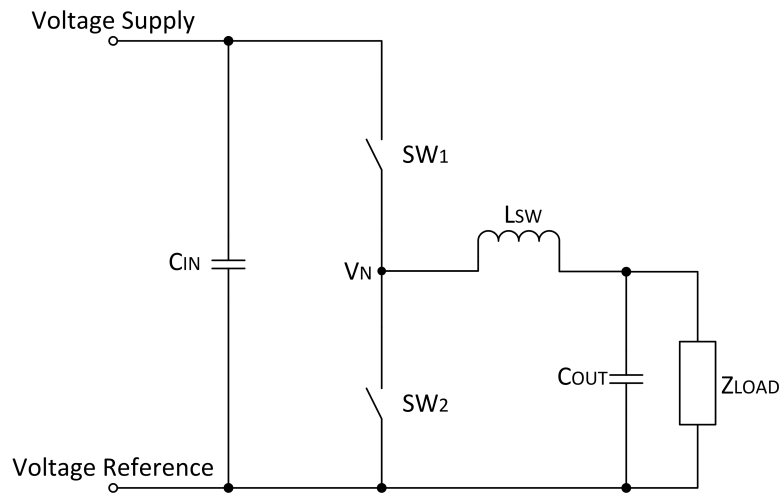


Figure 2.4. DC to DC Buck Switched-Mode Power Supply

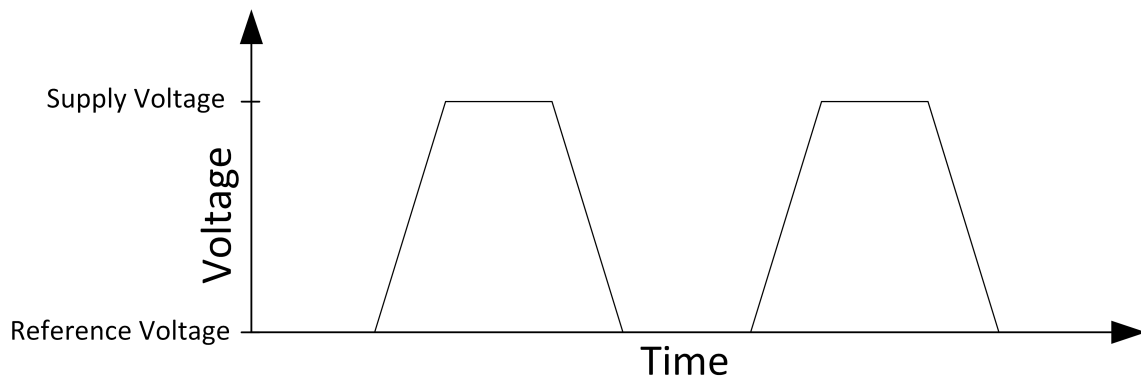


Figure 2.5. Switch Node Voltage for Switched-Mode Power Supply

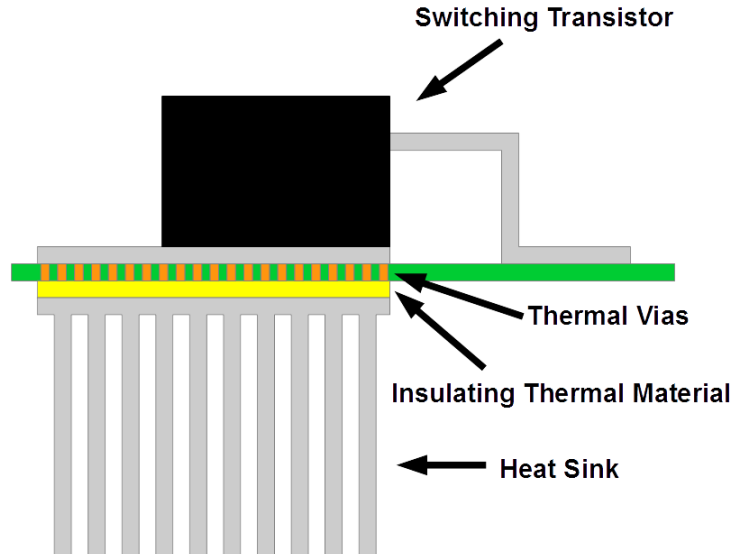


Figure 2.6. Heat Sink Cross Section

the V_N and the heat sink. This parasitic capacitance due to the heat sink is shown in Figure 2.7 [7].

Recalling the relationship between current and voltage of a capacitor from Equation 2.1, it can be seen that a current proportional to the switching time of SW_1 is displaced onto the heat sink. The current due to the parasitic capacitance from the heat sink can be the main source of EMI from an SMPS [2].

$$i(t) = C \cdot dv/dt \quad (2.1)$$

2.3.2. Equivalent Common Mode Noise Source Model

Using the information about how a CISPR 25 emissions test is set up and what one potential noise source from an SMPS looks like in a schematic, a common mode noise source model can be developed. For the purpose of this work, a common mode noise source is an unintended voltage that is referenced to chassis or earth ground. Figure 2.8 is a schematic of the CISPR 25 emissions setup with the previously mentioned buck SMPS.

If the assumption is made that C_{in} and C_{out} for the buck power supply are very low impedance at high frequencies, then they can be replaced with electrical shorts. Now, model-

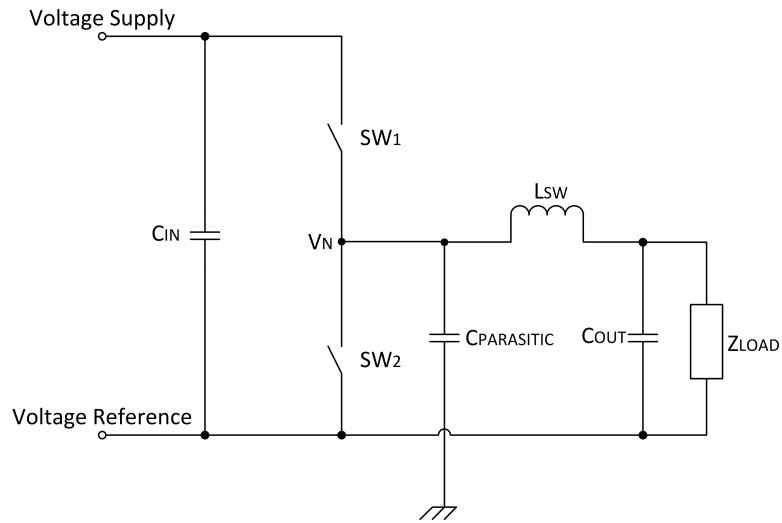


Figure 2.7. DC to DC Buck Switched-Mode Power Supply with Parasitic Heat Sink Capacitance

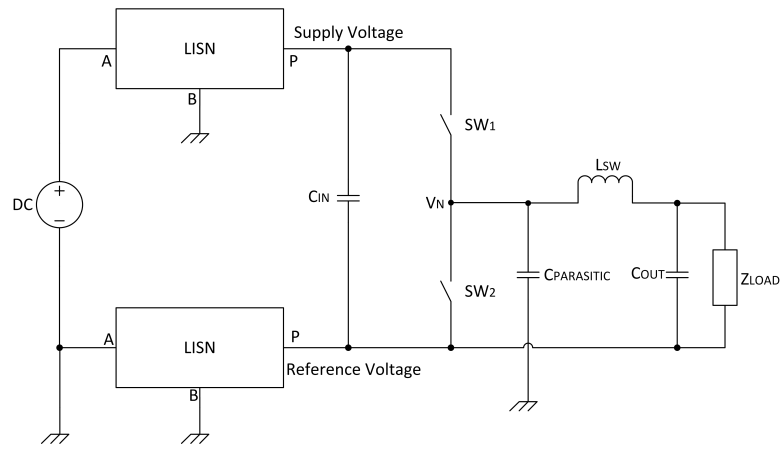


Figure 2.8. CISPR 25 Setup with DC to DC Buck Switched-Mode Power Supply

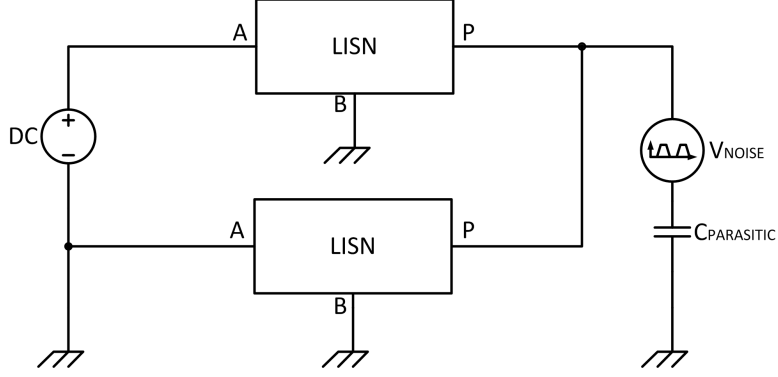


Figure 2.9. CISPR 25 Setup with an Equivalent Common Mode Noise Source Model

ing the switching node voltage as a trapezoidal voltage source allows for the removal of SW_1 , SW_2 , and L_{SW} . The adjusted common mode system schematic for a CISPR 25 test is given in Figure 2.9. The equivalent common mode noise source model of a trapezoidal voltage source in series with a capacitance to chassis for a buck SMSP will be used for the rest of this work.

2.4. Filtering

Filtering is a tried and true method for removing both common and differential mode noise from all sorts of circuits, not just power supplies. Filtering works to either impede the flow of noise current or shunt the noise current back to the noise source.

2.4.1. Definition of S21

To help compare different filter topologies and designs to each other a subset of the scattering matrix, S21 will be defined. For a filter, there will be a minimum of two ports, one port where the noise source is present, called port 1, and another port that is the output or load, called port 2. S21 is a measure of the voltage across port 2 relative the voltage cause by port 1. Mathematically S21 can be expressed in Equation 2.2 [8].

$$S21 = V_2/V_1 \quad (2.2)$$

Note that S21 will be equal to or less than 1 for passive systems. S21 is commonly expressed in terms of decibels (dB).

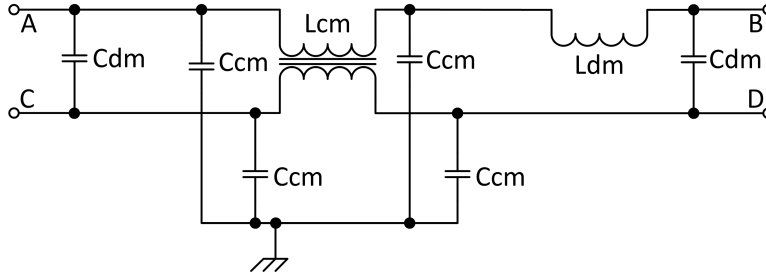


Figure 2.10. Traditional Power Supply Filter

2.4.2. Traditional Filtering

A traditional power supply filter for passing either a conducted or radiated emissions test is shown in Figure 2.10 [2, 3]. Topologies do vary, but the filter in Figure 2.10 has all of the traditional elements.

In a simple two conductor DC power feed there will be both a power supply line and power return. In Figure 2.10, the C_{dm} are capacitors for filtering differential mode noise on the power supply lines. Similarly, L_{dm} is an inductor also used for filtering differential mode noise on the power supply lines. The C_{cm} , are common mode capacitors used for filtering common mode noise on the power supply lines. C_{cm} differ from C_{dm} in that they are connected generally to a chassis or earth ground. Common mode capacitors are often limited in capacitance due to different design requirements, usually involving safety and needing to isolate the power supply lines from chassis or earth ground. L_{cm} is a common mode inductor, or a common mode choke, used for filtering common mode noise from the power supply lines. For a traditional power supply filter the common mode choke is often the largest component, due to the limited capacitance of the common mode capacitors. Depending on the power required and the frequency of suppression needed a costly custom common mode choke may be required. As SMPS continue to increase in frequency and in power, the common mode choke will continue to make up a large portion of the total system cost and size [9].

2.4.3. Active Filtering

In contrast to using a large traditional power supply filter, an active filter can be used to replace or supplement the existing common mode choke. As discussed in previous research, there are four basic topologies for active power supply filtering [10]: Current Sensing Current

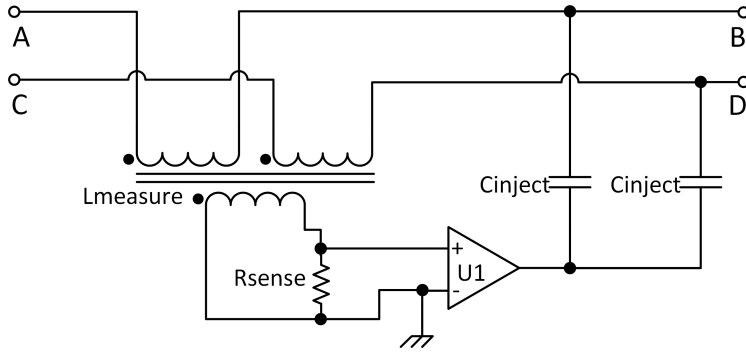


Figure 2.11. Current Sensing Current Adjusting Schematic

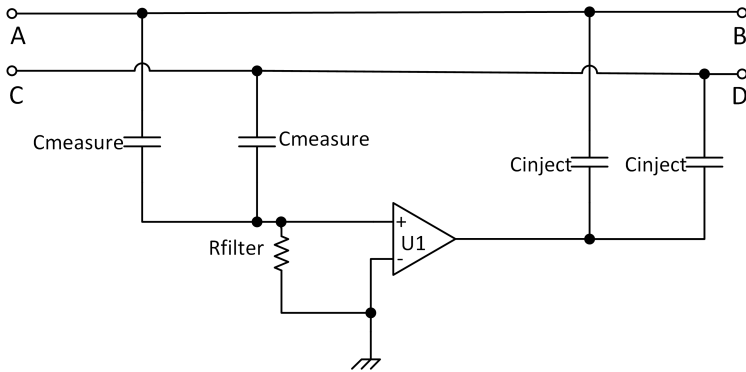


Figure 2.12. Voltage Sensing Current Adjusting Schematic

Adjusting (CSCA), Voltage Sensing Current Adjusting (VSCA), Current Sensing Voltage Adjusting (CSVA), and Voltage Sensing Voltage Adjusting (VSVA). Each topology has different advantages and disadvantages. A schematic of each topology is given in Figures 2.11, 2.12, 2.13, and 2.14 [11].

A main advantage of the voltage sensing architectures is that they do not require a current transformer on the power supply lines to measure the common mode current. Similarly the current adjusting architectures do not require a transformer on the power lines to inject the cancelation signal. Designing an active power supply filter that does not use a transformer is very desirable. Transformers can limit the possible bandwidth of the filter due to parasitic capacitance between the windings. A filter without a transformer could be designed in such a way that the designed circuit is independent of the amount of differential mode current flowing on the power supply lines. A transformerless design allows for a smaller size and a lower impact on the power supply lines.

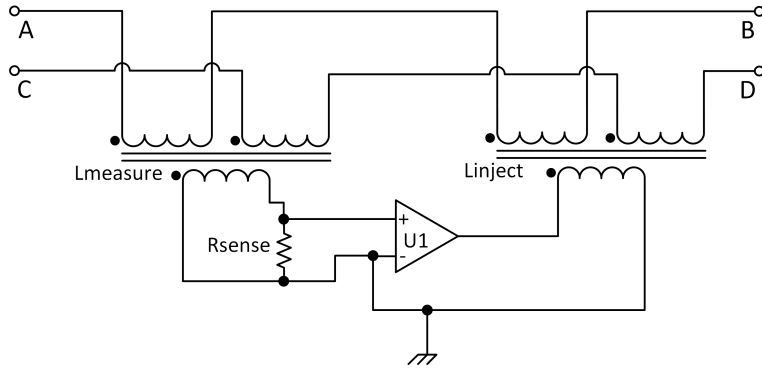


Figure 2.13. Current Sensing Voltage Adjusting Schematic

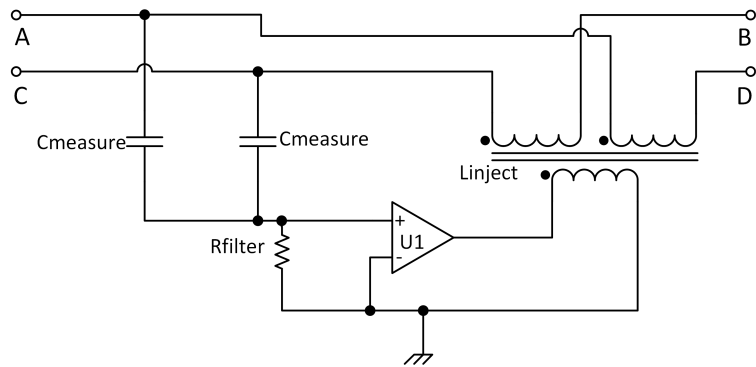


Figure 2.14. Voltage Sensing Voltage Adjusting Schematic

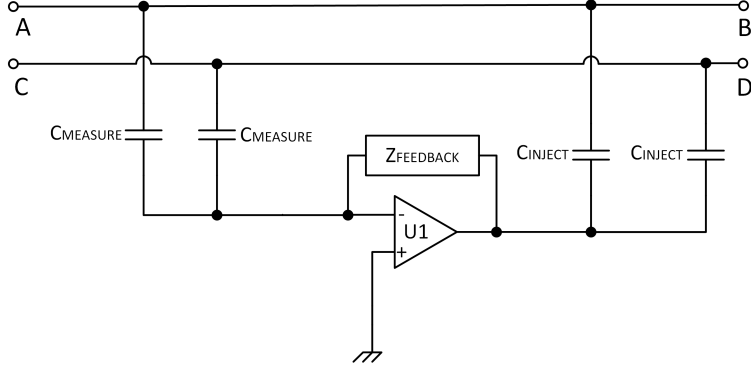


Figure 2.15. Proposed Voltage Sensing Voltage Adjusting Schematic

2.4.4. Voltage Sensing Current Adjusting Architecture

Previously, the work in [11] examined a transformerless active filter designed to operate in the region between 150kHz-30MHz. It showed that a transformerless design can be stable over a very large range of both source and load impedances. To achieve filtering above 2MHz, the design reported in [11] used passive components and did not rely on the active circuit. Similarly, the work reported in [12] also designed a transformerless active filter. They showed that a great amount of cost savings and size reduction can be achieved using an active filter. Again though, their maximum active filter frequency was limited to 2MHz.

A schematic of a potential VSCA filter for use with a DC to DC SMSP is given in Figure 2.15. Notice the voltage measuring stage of the filter consists of two capacitors, C_{measure} . These capacitors block any DC voltage and allow common mode AC noise to pass to the inverting input of the amplifier. The amplifier then uses the feedback network, Z_{feedback} , to create a cancellation signal, and injects that signal into the power supply lines through C_{inject} . C_{inject} also serves the purpose of protecting the output from the DC voltage on the supply lines.

Note that in this design, the non-inverting input of the amplifier is connected to the chassis. To help satisfy any potential safety concerns, it is important that the amplifier be powered from isolated power supplies and the capacitors in the circuit be safety rated Y capacitors. A Y capacitor is a special type of high reliability capacitor that is designed to fail open rather than fail short. This helps to protect consumers from the potentially dangerous power supply voltage in case of failure.

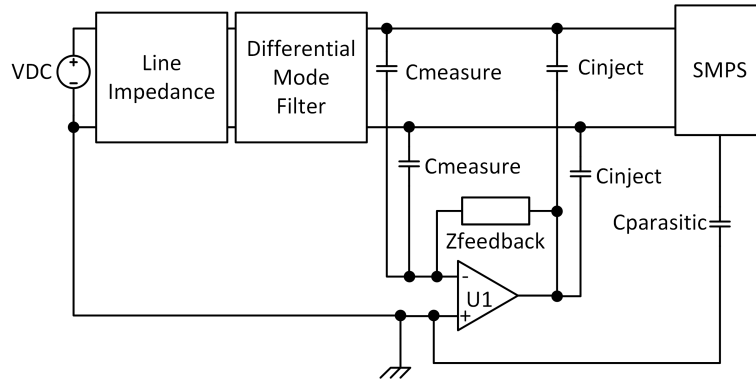


Figure 2.16. VSCA Filter in System Application

To balance the common mode correction signal properly, it is important that C_{inject} be the same capacitance value and low tolerance. Any mismatch in the injection capacitors will cause error in the output. Optimal values for these capacitors and other components for the circuit given in Figure 2.15 will be presented in Chapter 3.

Careful examination of the circuit in Figure 2.15 will reveal that any high frequency differential mode voltage noise on the power supply lines will be presented at the non-inverting of the amplifier. In order to prevent the filter from measuring and responding to high frequency differential mode noise, a high frequency differential mode filter should be added before the input of the VSCA filter. A block diagram of schematic of a system using this VSCA filter is given in Figure 2.16. It is worthwhile to note that a practical SMSP design will already contain a differential mode filter for the power supply lines. The differential mode filter is given in Figure 2.7 as C_{in} .

CHAPTER 3. RESULTS

3.1. Introduction

Chapter 3 discusses one potential solution to the problem of conducted and radiated emissions presented in Chapter 2. The proposed filter at the end of Chapter 2 is expanded upon, analyzed, and synthesized. Simulations are conducted to predict real world performance. S21, frequency domain, and time domain measurements of a test filter with several possible feedback configurations are presented.

3.2. Analysis of Proposed Active Filter

To begin analyzing the VSCA active filter proposed in Chapter 2, it will first be assumed that the noise source the circuit is trying to filter is the common mode noise from a SMPS. The combined circuit of Figure 2.15, the equivalent common mode noise source of a SMPS, and a common mode load is shown in Figure 3.1. The equivalent common mode noise source impedance is labeled as Z_{source} in Figure 3.1. The common mode load, Z_{LISN} , represents the LISNs used as part of the measurement setup in a standard test, such as CISPR 25.

3.2.1. Transfer Function

Using nodal analysis and the properties of an ideal op-amp, a function for voltage across $Z_{\text{LISN}}(s)$ from the circuit shown in Figure 3.1 was derived and is given in 3.1. This transfer function can be used to help find the ideal feedback network with an ideal op-amp. Using 3.1, assuming a source impedance, $Z_{\text{source}}(s)$, of a 200pF capacitor in series with 50Ω resistor, and a 50Ω LISN impedance, the voltage across Z_{LISN} is plotted using MATLAB in Figure 3.2 a feedback network in which Z_{feedback} is 1GΩ, a feedback network in which Z_{feedback} is 0Ω and a feedback in which Z_{feedback} is 100Ω. Figure 3.2 shows that a 1GΩ feedback network should have the lowest voltage across the LISN, while a 0Ω feedback network is has a similar voltage across the LISN as a 100Ω feedback up until about 2MHz. After 2MHz the 100Ω feedback outperforms the 0Ω feedback network. For all of the MATLAB calculations C_{measure} and C_{inject} were taken to be 1nF capacitors.

3.2.2. Determination of Z_{feedback}

From 3.1 it can clearly be seen that the best feedback configuration for the ideal op-amp is when the feedback network is open. Examining 3.1 shows that this makes sense. The lowest

$$\frac{V_{LISN}(s)}{V_{source}(s)} = \frac{1}{\left(\frac{1}{Z_{source}(s)} + \frac{2}{Z_{measure}(s)} + \frac{2}{Z_{inject}(s)} + \frac{4 \cdot Z_{feedback}(s)}{(Z_{measure}(s) * Z_{inject}(s))} + \frac{1}{Z_{LISN}(s)} \right)} \cdot \frac{1}{Z_{source}(s)} \quad (3.1)$$

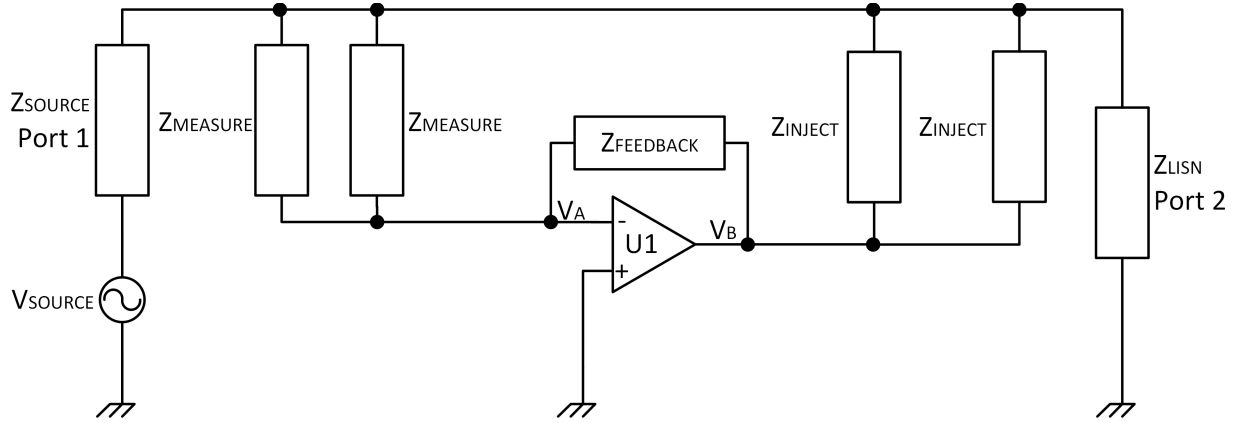


Figure 3.1. System schematic with proposed VSCA filter for analysis

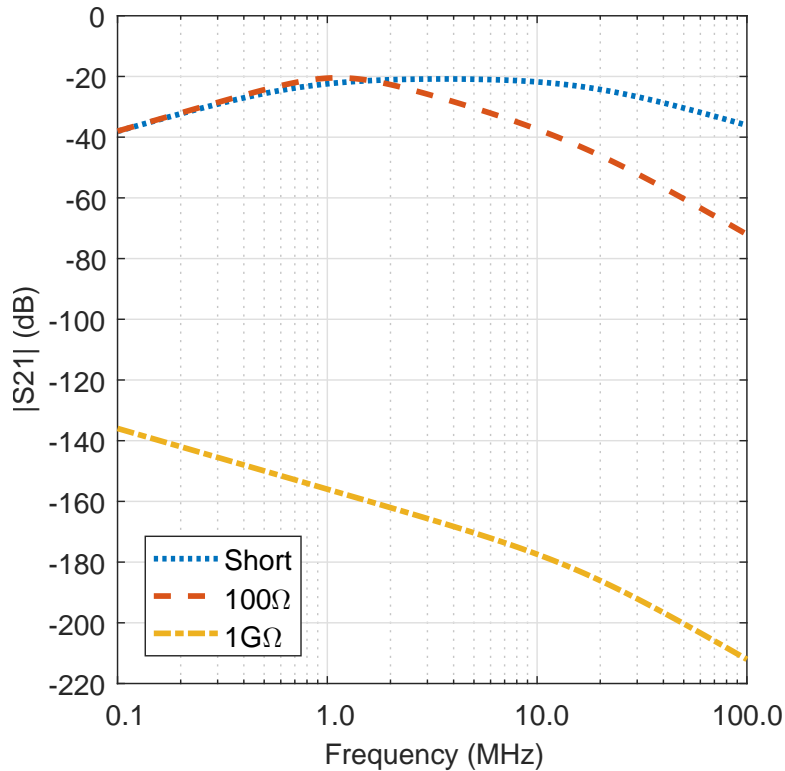


Figure 3.2. MATLAB plot of voltage across the LISN impedance predicted by 3.1 using three possible feedback configurations, a shorted feedback network, a 100Ω feedback network, and a 1GΩ feedback network.

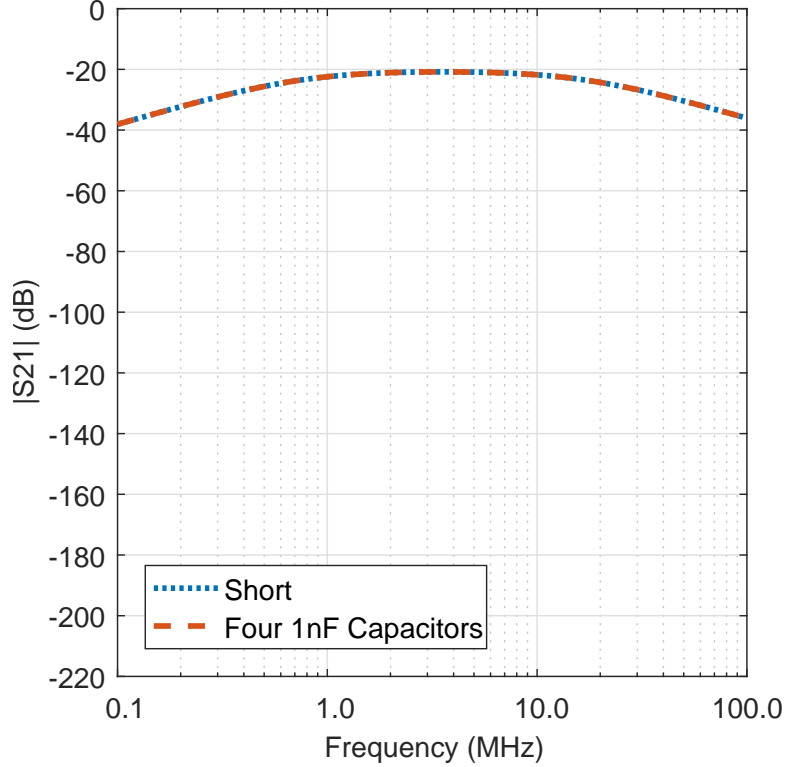


Figure 3.3. MATLAB plot comparing four 1nF capacitors connected in parallel with Z_{LISN} to proposed filter with shorted feedback.

common mode voltage across the LISN will be as $V_{\text{LISN}}(s)/V_{\text{source}}(s)$ approaches zero. By holding all other values constant, the best way to get $V_{\text{LISN}}(s)/V_{\text{source}}(s)$ to approach zero is to increase $Z_{\text{feedback}}(s)$. For an ideal op-amp, the best feedback network is an open circuit.

Contrastingly, examining 3.1 shows the worst performing feedback network is a short circuit. Again this result makes intuitive sense. For an ideal op-amp, the output of op-amp would simply be the chassis reference voltage at the inverting input, since the output and the non-inverting input are tied together. In essence this feedback network does not take advantage of the voltage gain the amplifier can provide. While the current flowing to the chassis is relatively small for the filter circuit with a shorted feedback network, the calculated voltage across Z_{LISN} is the same as connecting 2 C_{measure} and 2 C_{inject} capacitors to chassis reference. This result is shown in Figure 3.3, where a comparison of an ideal short feedback network with an ideal op-amp is compared to a filter with four 1nF filtering capacitors.

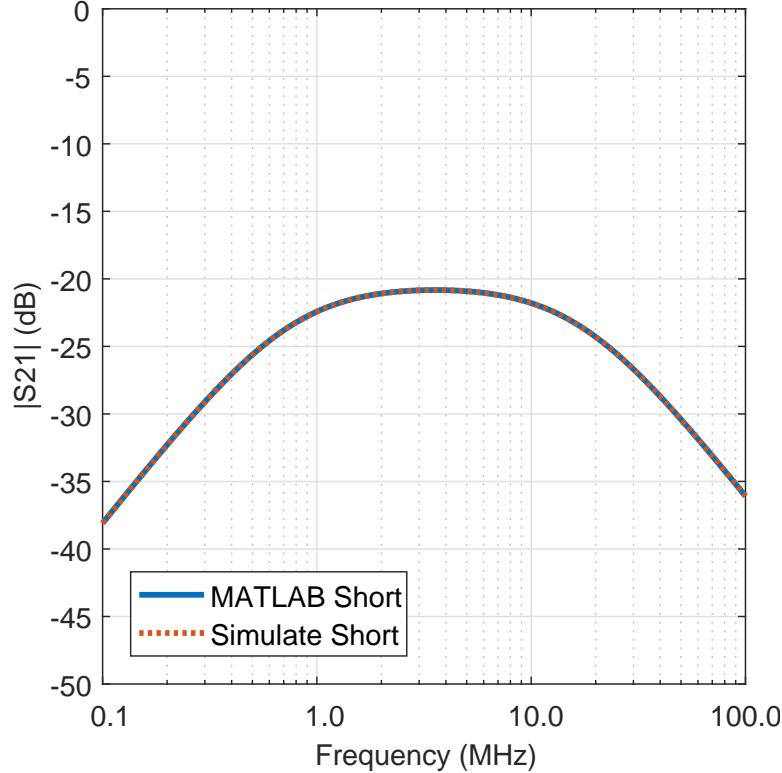


Figure 3.4. Plot of S21 comparing MATLAB code using 3.1 to Keysight ADS simulation using ideal an op-amp and a shorted feedback network.

3.2.3. Ideal Simulation

As part of the design, the circuit was simulated using Keysight’s ADS 2015 [13]. First the circuit was simulated using an ideal op-amp model. For the simulation an S-parameter sweep was conducted. The results for an ideal op-amp with a shorted feedback network are given in Figure 3.4 and are compared to the MATLAB results given for 3.1. Similarly, the results for a simulation with a 100Ω feedback network are given in Figure 3.5. Finally, the results for a simulation with an open feedback network are given in Figure 3.6, where the MATLAB comparison uses a feedback resistor of $1G\Omega$. From Figures 3.4, 3.5, and 3.6, it is shown that ADS simulation with and ideal op-amp closely matches the MATLAB results for 3.1. The only noticeable difference is that the open configuration does not filter as much as the $1G\Omega$ feedback. This is a result of the op-amp in ADS having a gain of 10,000 and an ideal op-amp having an infinite gain.

3.2.4. Bandwidth Limited Simulation

Next, simulations were done with a non-ideal, bandwidth limited op-amp. Figure 3.7 shows the simulation schematic in ADS with a 100Ω feedback network. For these simulations a 400MHz

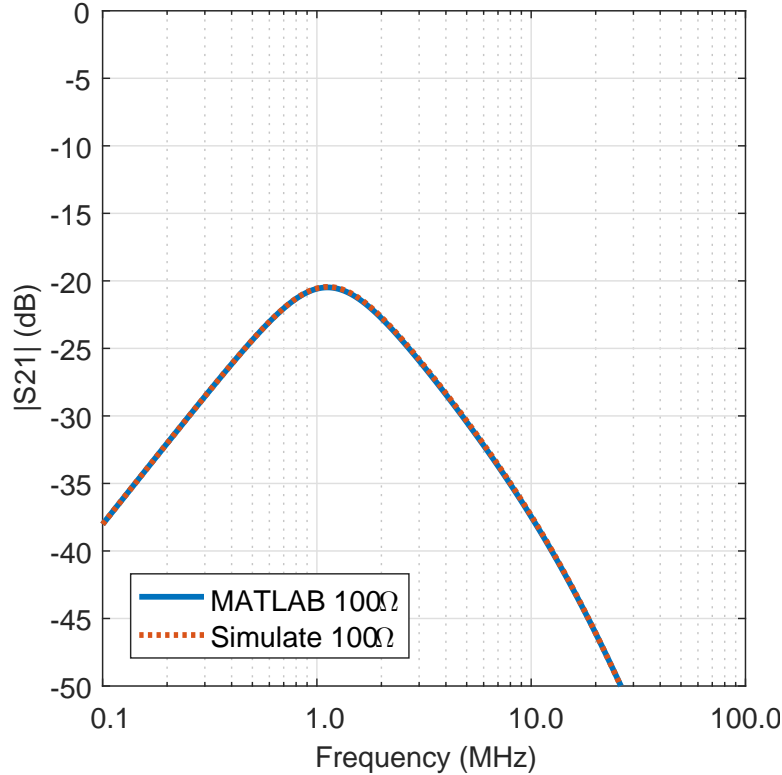


Figure 3.5. Plot of S21 comparing MATLAB code using 3.1 to Keysight ADS simulation using ideal an op-amp and a 100Ω feedback network.

bandwidth was selected for the bandwidth limited model and a slew rate of $950\text{V}/\mu\text{s}$ were used. The gain on the op-amp was set to 60dB. Using an S-parameter sweep the results for a shorted feedback network, a 100Ω network, and an open feedback network are given in Figure 3.8.

The results of the bandwidth limited simulation are interesting because they begin to show how a bandwidth limited op-amp will respond. Comparing the 100Ω feedback network bandwidth limited simulation and MATLAB results using 3.1 are done in Figure 3.9. From the graph it can be seen that the non-ideal bandwidth limited op-amp has more loss than the results predicted by 3.1 between 10MHz and 24MHz. This effect wears off as frequency increases and the bandwidth limited amplifier is out performed by 3.1 after 24MHz.

Looking more closely at the differences between the ideal and bandwidth limited op amp circuits with a 100Ω feedback network, a comparison of the voltage magnitude on the output of the op amps is given in Figure 3.10. The voltage magnitudes look to match very closely, the differences in the S21 simulated values does not appear to be explained by the magnitude of the voltage output by the op amps.

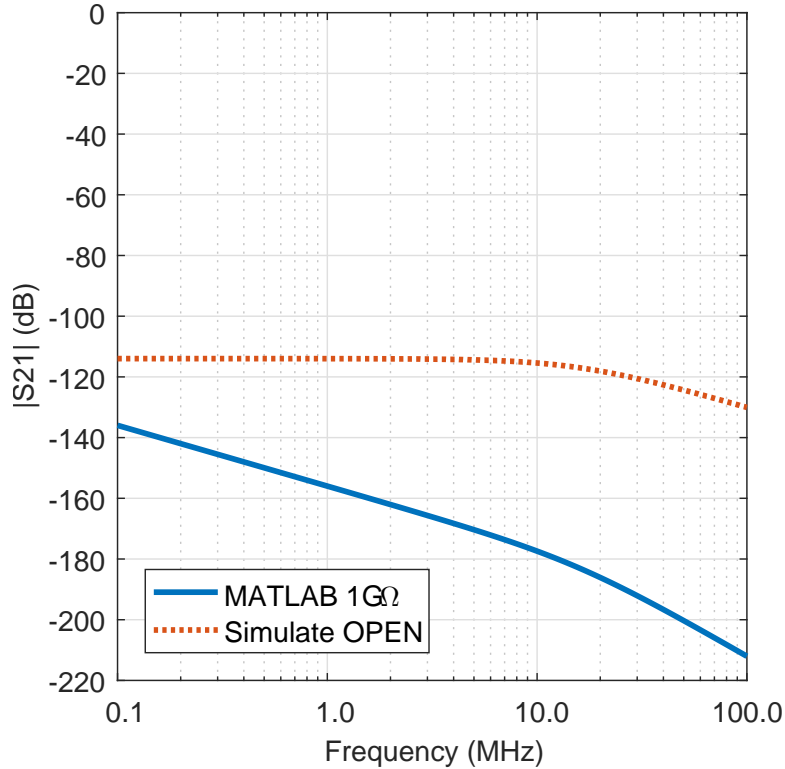


Figure 3.6. Plot of S21 comparing MATLAB code using 3.1 with $1\text{G}\Omega$ feedback network to Keysight ADS simulation using an ideal op-amp with a gain of 10000 and an open feedback network.

Figure 3.11 is a voltage phase plot comparing the op amp outputs over frequency for the 100Ω feedback network. The phase difference shows that the bandwidth limited op amp is not able to keep up with the ideal op amp. This causes a lagging phase, and it appears to be this phase difference that causes the bandwidth limited op amp to outperform the ideal op amp up to a certain frequency. As frequency continues to increase the bandwidth limited amplifier continues to have its output lag and eventually the ideal op amp outperforms it.

Exploring the difference between the ideal and the bandwidth limited model for the op-amp shows the limitation of 3.1. The effect of op-amp bandwidth is reinforced in Figure 3.12, where the 100Ω feedback circuit is simulated with multiple bandwidths (100MHz, 200MHz, and 400MHz). From Figure 3.12 shows that selecting an op-amp with higher bandwidth should filter out higher frequencies.

3.3. Filter Synthesis

The op-amp selected for this circuit was a Texas Instrument's THS4271. The THS4271 was selected because of its large bandwidth (380MHz), dual 5V supply rail operation, and its low output

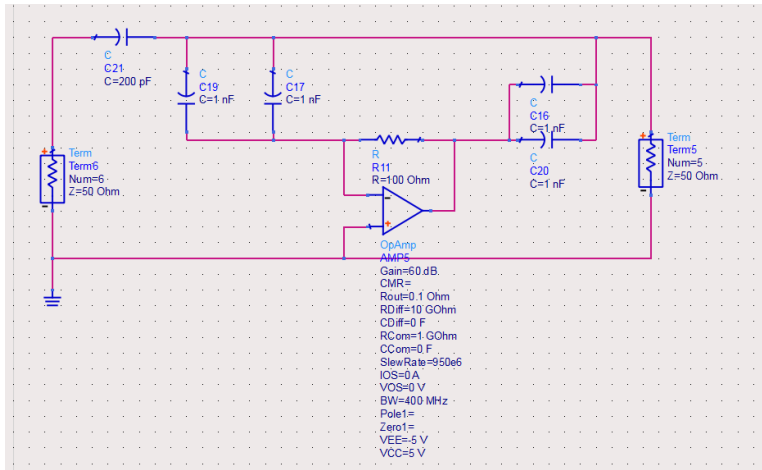


Figure 3.7. Bandwidth limited simulation circuit schematic in Keysight's ADS 2015.

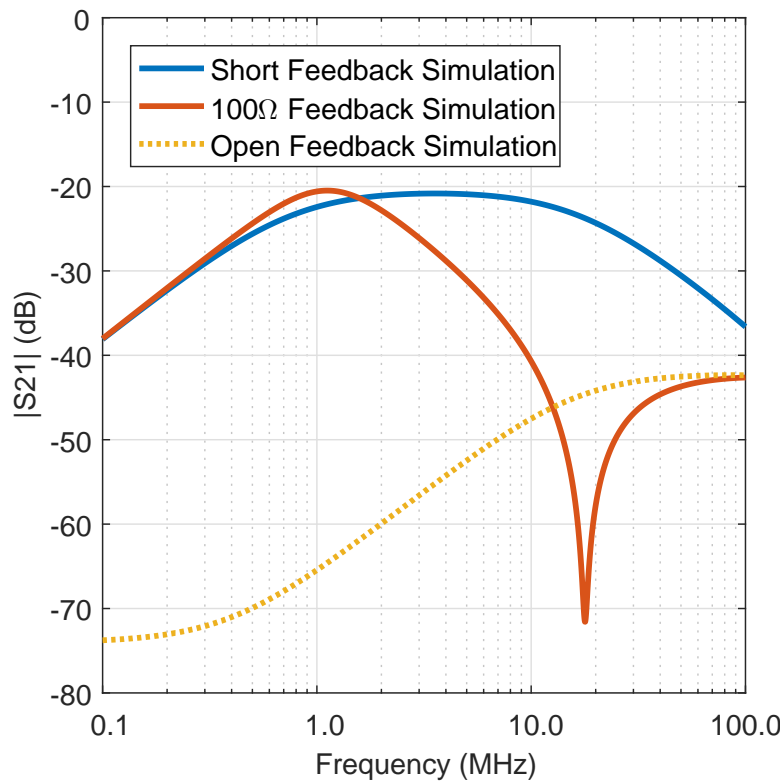


Figure 3.8. S21 Bandwidth limited circuit simulation results using three different feedback network configurations: a shorted feedback network, a 100Ω network, and an open feedback network. The op amp was set to have a bandwidth of 400MHz.

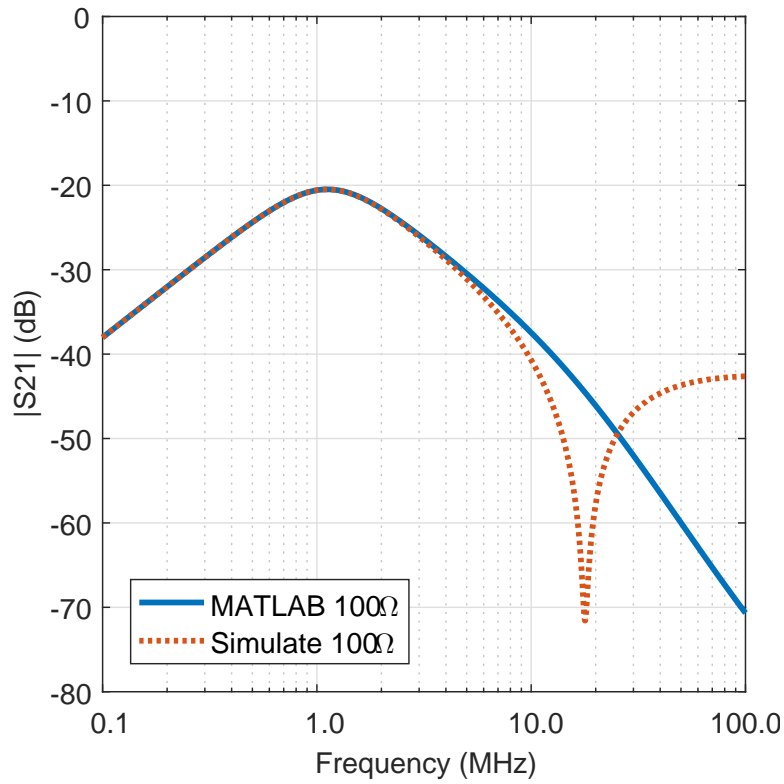


Figure 3.9. Results of S21 bandwidth limited circuit simulation with 100Ω feedback compared to MATLAB predicted results using 3.1 with a 100Ω feedback configuration.

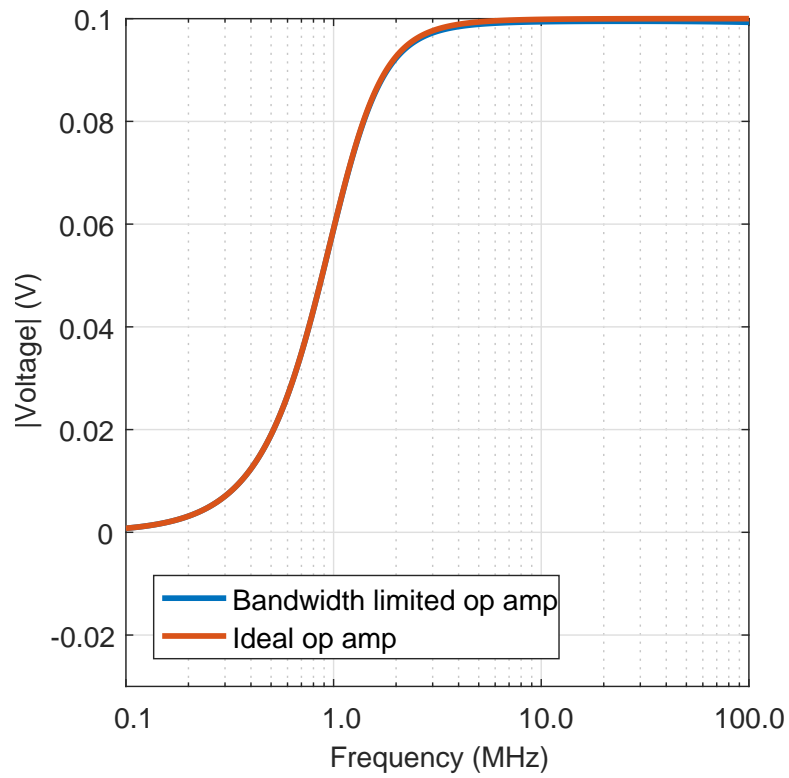


Figure 3.10. Voltage magnitude at output of op amp for both an ideal and bandwidth limited circuit simulation with 100Ω .

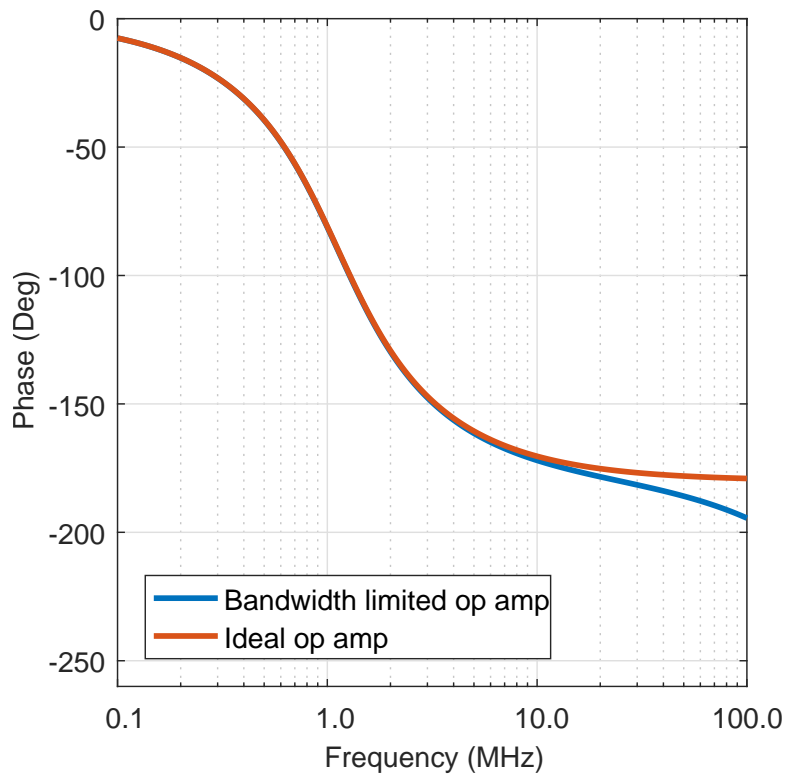


Figure 3.11. Voltage phase at output of op amp for both an ideal and bandwidth limited circuit simulation with 100Ω .

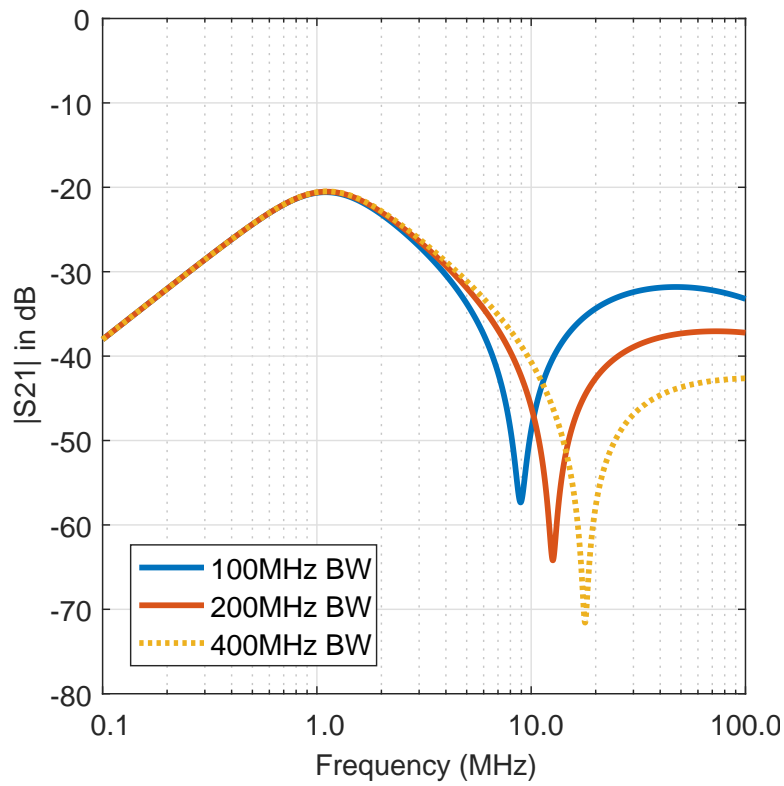


Figure 3.12. Circuit simulation with 100Ω feedback and a bandwidth limited op-amp with three different bandwidths, 100MHz, 200MHz, and 400MHz.

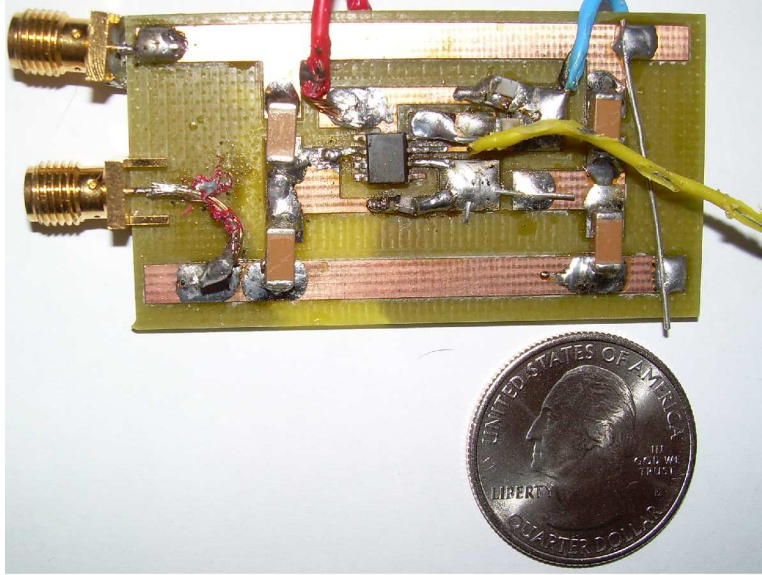


Figure 3.13. Photo of designed circuit. A quarter is given for size comparison.

impedance [14]. The op-amp was supplied with a +5V and -5V power rail and was decoupled with a $0.1\mu\text{F}$ capacitor on the power supply input pins. The large bandwidth of the op-amp was selected to be sure that the frequency response does not roll off before our desired cut-off frequency. The circuit was built on a printed circuit board and is pictured in Figure 3.13. For the circuit a variety of feedback networks were tested, but C_{measure} and C_{inject} were taken to be 1nF Y-rated capacitors. A full schematic of the designed filter circuit is given in Figure 3.14. The differential mode capacitors (C5-C8) were 1nF capacitors.

3.4. Measurements

3.4.1. S21 Measurement

For the S21 measurements Keysight's E5071C Network Analyzer was used. The power level on the network analyzer was set to 10dBm and the circuit was powered by +5V and -5V. A schematic of the test setup is given in Figure 3.15. First the circuit with three different feedback networks were measured. The feedback networks included a shorted feedback network, a feedback network with a 100Ω resistor, and an open feedback network. In addition, a circuit consisting of four in parallel 1nF capacitors connected to chassis was also measured. These measurements are given in Figure 3.16.

The S21 measurements show a variety of interesting phenomenon. First it is interesting to see that the S21 measurement for the filter with the open feedback network differs greatly from the

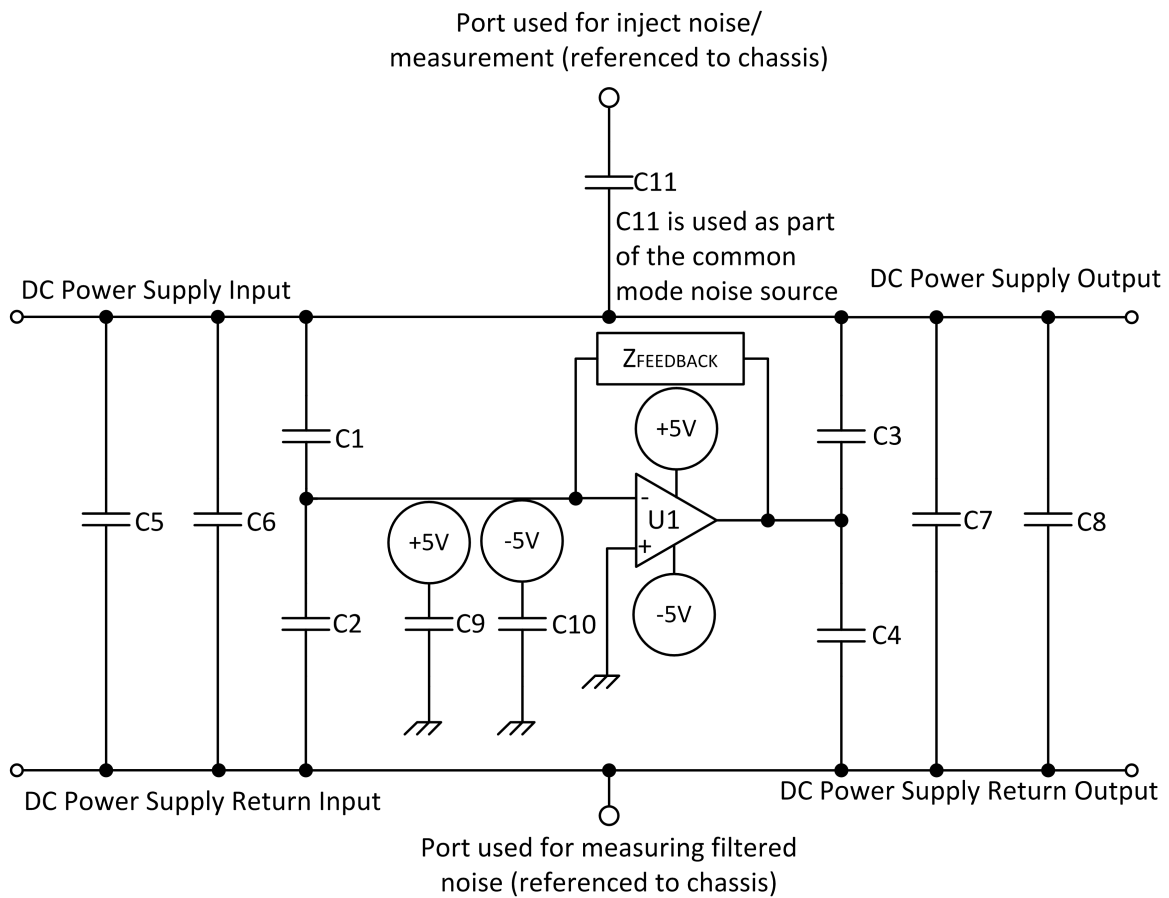


Figure 3.14. Schematic of synthesized circuit, TI's THS4271 was used for U1.

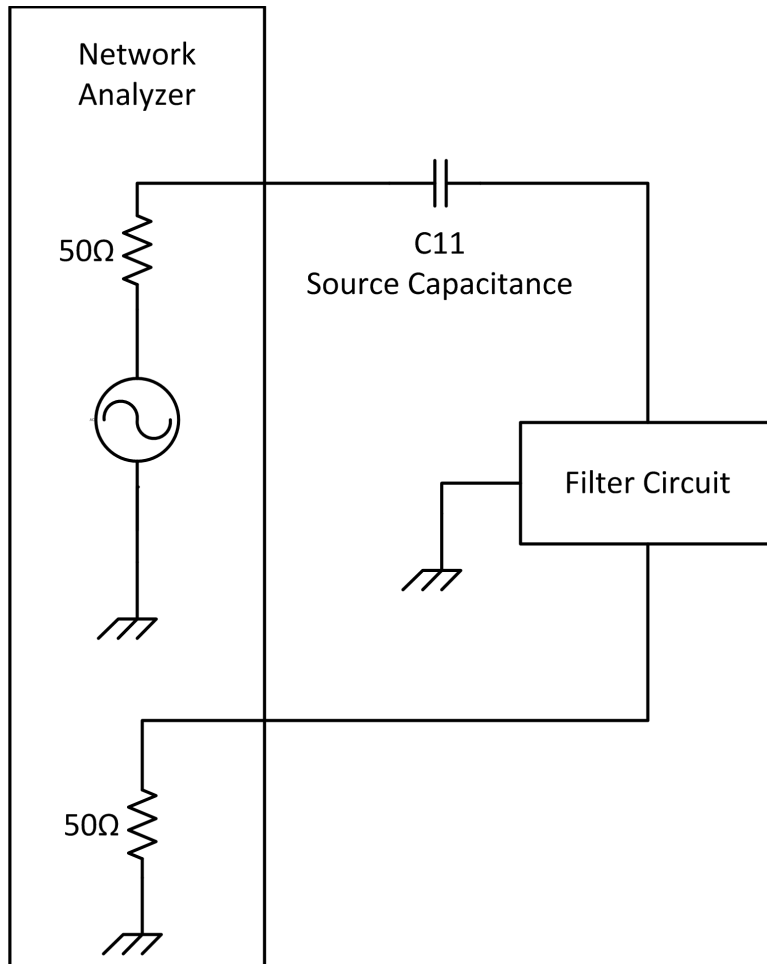


Figure 3.15. Test Setup for S₂₁ Measurements

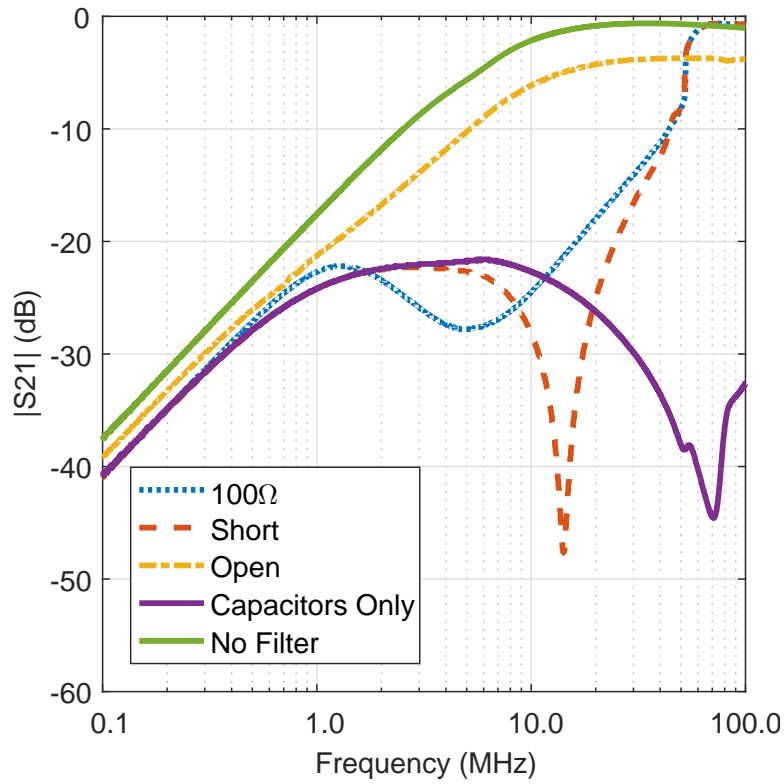


Figure 3.16. Plot of S_{21} with a 10dBm source applied to circuits under test with a 50Ω resistor in series with a 220pF capacitor as source impedance. The test circuit uses three different possible feedback networks, a shorted network, an open network, and an open circuit network. The plot compares the active filter to four 1nF capacitors and a setup with no filter present.

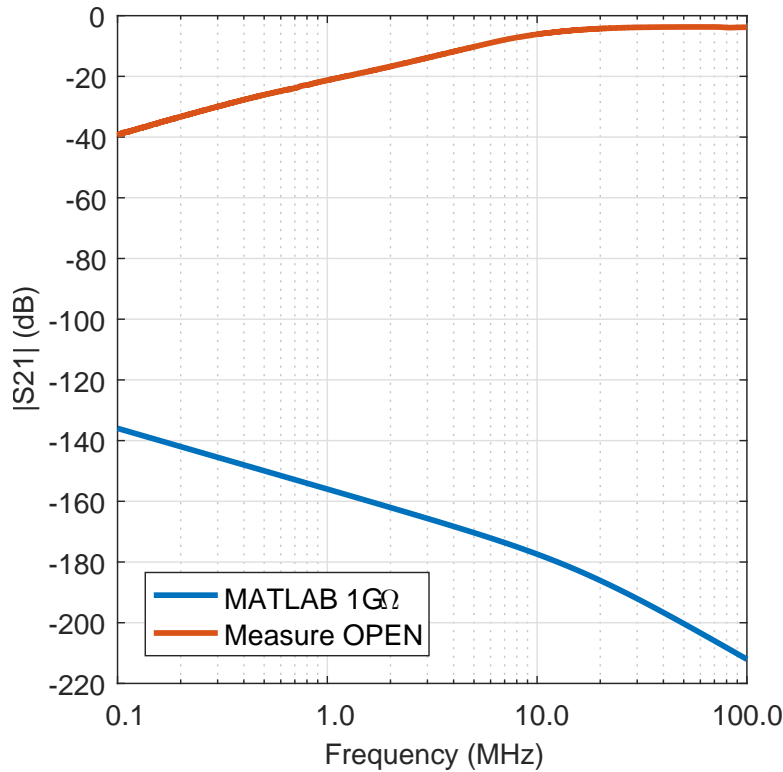


Figure 3.17. Plot of measured S21 of test circuit with an open feedback configuration compared to MATLAB code using 3.1 with a $1\text{G}\Omega$ feedback network.

MATLAB calculated values. A comparison is shown in Figure 3.17. There is a variety of reasons why this may occur, such as the infinite gain assumed by 3.1, but the exact explanation for it is beyond the scope of this project.

Next it is interesting to see that the S21 measurement for the filter with the 100Ω matches the MATLAB calculated values until about 4MHz. A comparison is shown in Figure 3.18. After 4MHz the limitations of the bandwidth limited op-amp begin to increase the S21 for the practical circuit. This is shown also in the simulation results for the 100Ω feedback network. At first it may seem confusing that the op-amp with bandwidth of 380MHz stops behaving as an ideal op-amp at 4MHz, but the op-amp's bandwidth also determines the phase characteristics of the output. Since the 400MHz bandwidth for the THS4271 is actually a 3dB, the phase in the output begins shifting at least a decade before the rated bandwidth of the op-amp. This small shift in phase begins to create an error term that increases with frequency and results in the phenomenon that shows the measured S21 results being higher than the MATLAB predicted S21 in Figure 3.18.

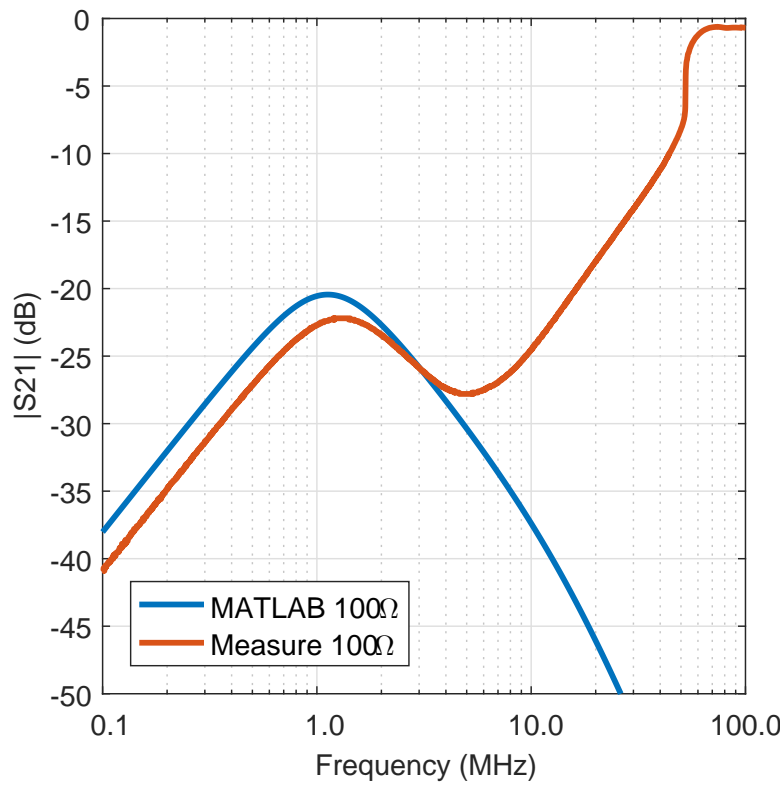


Figure 3.18. Plot of measured S21 of test circuit with a 100Ω feedback configuration compared to MATLAB code using 3.1 with a 100Ω feedback network.

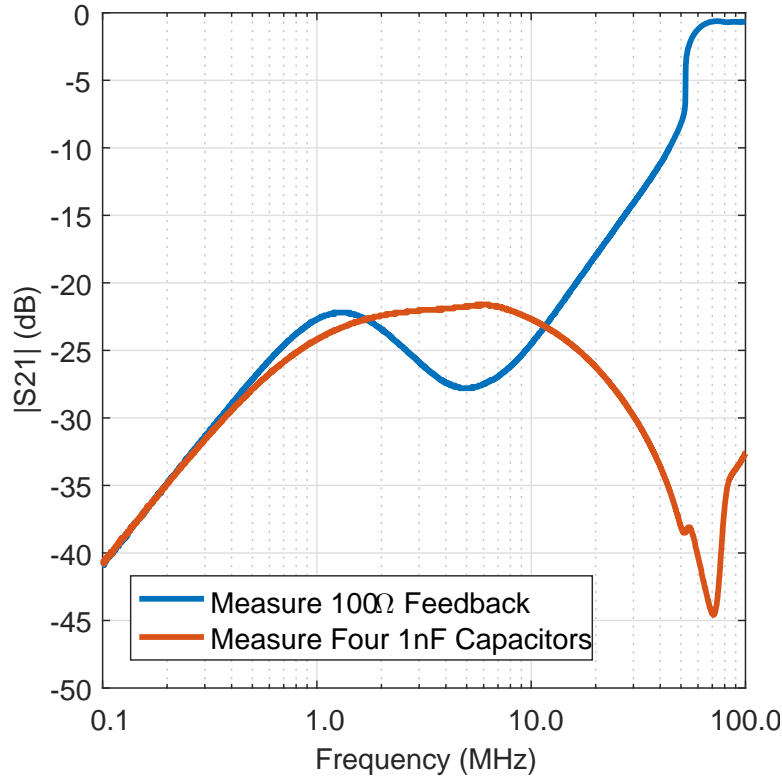


Figure 3.19. Plot of measured S21 of test circuit with a 100Ω feedback configuration compared to measured S21 of circuit using four 1nF capacitors connected in parallel.

Also it is interesting now to compare the filter with 100Ω feedback to the measured value of four 1nF capacitors. A plot of this is given in Figure 3.19. From the plot it can be seen that the active filter performs better than a strictly passive filter from roughly 2MHz to 10MHz . From Figure 3.19 the largest difference was found to be about 6dB .

Finally, the filter measurements with the shorted feedback network will be compared to the original MATLAB code. A comparison of the measurement to the MATLAB values is given in Figure 3.20. The measurements agree closely with the original MATLAB code up until about 7MHz . After 7MHz the bandwidth limitations of the op-amp again take over and it can be seen that they decrease the S21 until about 15MHz and then the S21 begins increasing again. The reasoning for this phenomenon is the same as the for the 100Ω feedback case.

Again it is worthwhile to compare the measured results of the circuit with a shorted feedback network to the measured results of the circuit with four 1nF capacitors. These are compared in Figure 3.21. Comparing the measurements shows that the shorted feedback network provides a greater loss than the purely passive filter between 4MHz and 20MHz , the greatest difference is

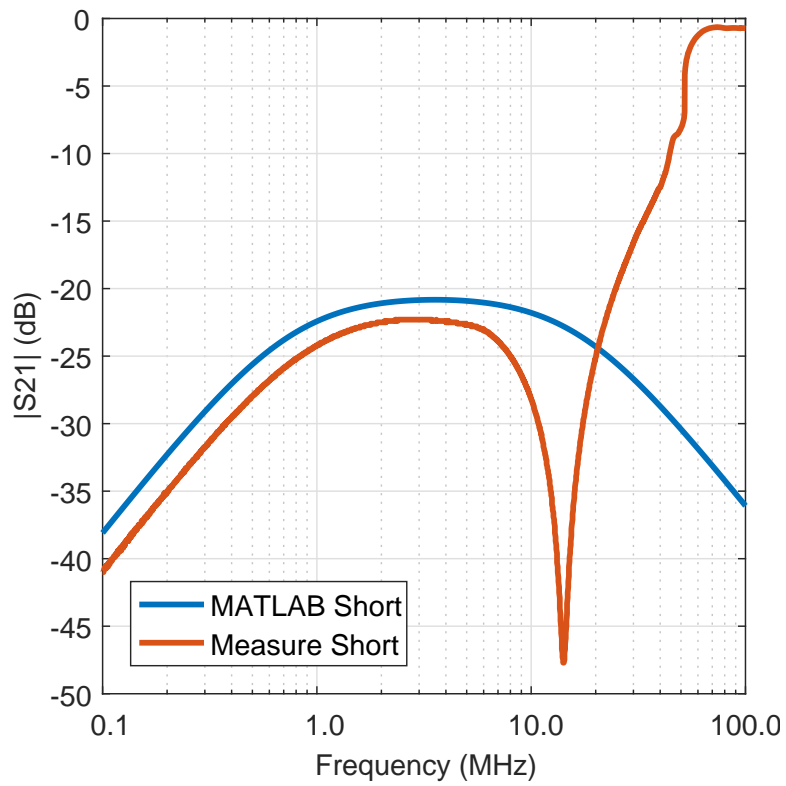


Figure 3.20. Plot of measured S21 of test circuit with a shorted feedback configuration compared to MATLAB code using 3.1 with a shorted feedback network.

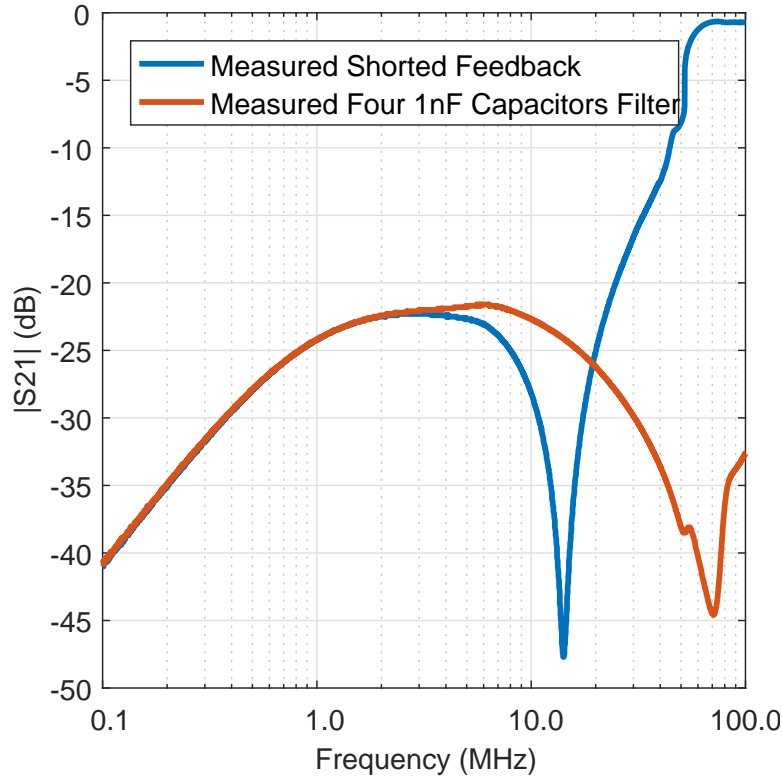


Figure 3.21. Plot of measured S21 of test circuit with a shorted feedback configuration compared to measured S21 of circuit using four 1nF capacitors connected in parallel.

measured to be 25dB. This is a very large difference that shows promise for the active filter in this frequency range.

It is prudent now to compare the difference between the 100Ω and the shorted feedback network. A comparison is given in Figure 3.22. Both configurations have a considerably large range of frequencies where they perform better than a purely passive filter. It is interesting to note how the 100Ω feedback appears to shift the active filter band lower while also decreasing the filter's maximum effectiveness. This seems to indicate that different resistor values could be used to tune the filter to filter specific frequencies between 2MHz and 14MHz.

3.4.2. Frequency Domain

For the frequency domain measurements the circuit was driven by Keysight's 81160A Pulse Function Arbitrary Generator, set to output a 50% duty cycle 3V peak to peak 1MHz square wave with 1ns rise and fall times. The spectral measurements were taken with Keysight's E4402B Spectrum Analyzer. The setup for frequency domain measurements are shown in Figure 3.23.

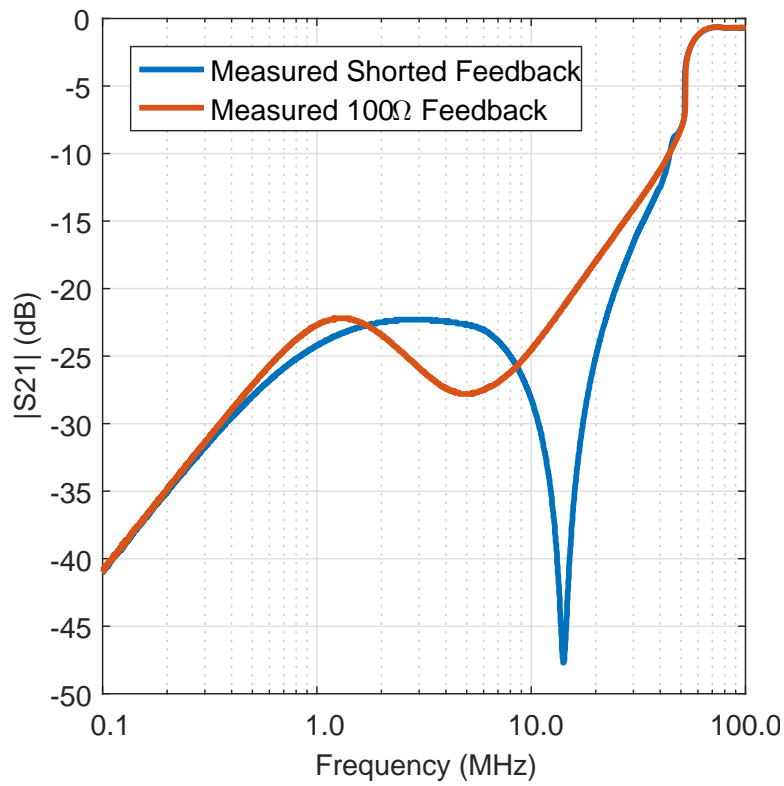


Figure 3.22. Plot of measured S_{21} of test circuit with a shorted feedback configuration compared to measured S_{21} of test circuit using a 100Ω feedback configuration.

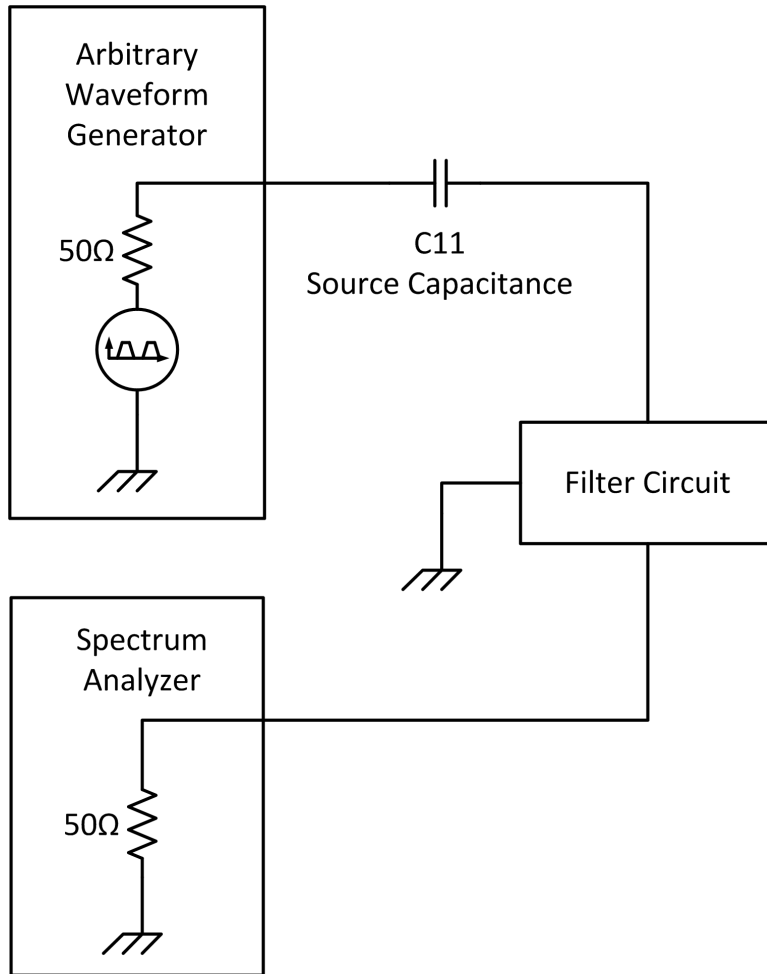


Figure 3.23. Test setup for time and frequency measurements.

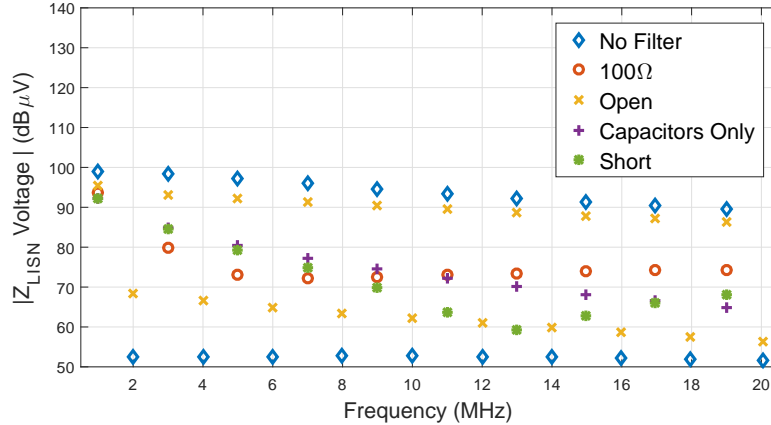


Figure 3.24. Plot of spectral measurements with a 1MHz square wave applied to circuits under test with a 50Ω resistor in series with a 220pF capacitor as source impedance. The input waveform was 3V peak to peak. The proposed filter circuit was tested with a shorted feedback configuration, 100Ω feedback configuration, and open feedback configuration. The proposed filter measurements are also compared to four 1nF capacitors in parallel and a test setup without a filter.

Similar to the S_{21} measurements, three different feedback networks were measured. The feedback networks included a shorted feedback network, a feedback network with a 100Ω resistor, and an open feedback network. Again, a circuit consisting of four in parallel 1nF capacitors and connected to chassis was also measured. The results between 500kHz and 20.5MHz are shown in Figure 3.24.

Figure 3.24 shows that the active filter performs significantly better than using four capacitors for common mode filtering at some frequencies in the 1MHz to 20MHz band. Interestingly, while the open feedback network was thought to be the best from a theoretical standpoint, when tested with an actual noise input, it provided less than 4dB of filtering over not using any filter. Additionally the open feedback configuration actually increased the levels of the even harmonics and caused the design to become more noisy. Based on these results, using an open feedback configuration would not be recommended. The 100Ω feedback configuration outperformed the four 1nF capacitors from 3MHz to 9MHz . This agrees with the S_{21} results showing that the feedback configuration outperformed the four 1nF capacitors between 2MHz and 10MHz . Looking at the performance of the shorted feedback network, the shorted feedback network outperforms the four 1nF capacitors from 7MHz until 17MHz . Note that now a difference is seen between the S_{21} measurements and the frequency domain measurement. Specifically at 19MHz the active filter

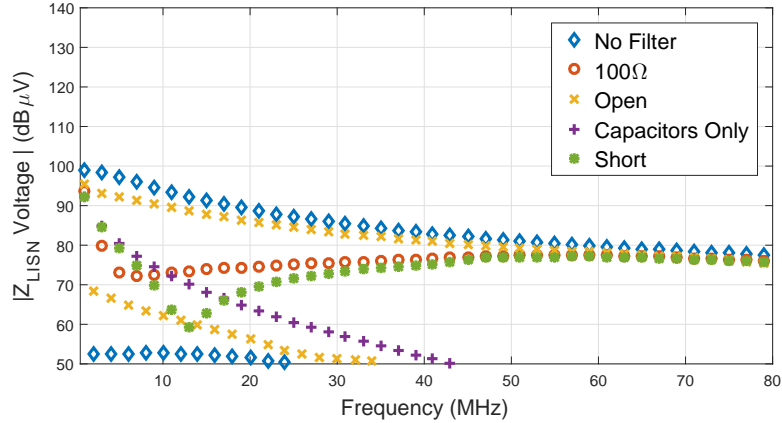


Figure 3.25. Plot of spectral measurements using the same setup as Figure 3.24, except with a larger frequency band shown.

measurement is a couple of dB higher than the four 1nF capacitors. This is important information to consider when designing an active common mode filter.

Figure 3.25 shows the response of the filter at frequencies even higher than 20MHz. The limitations of an active filter become very evident. After 20MHz the four 1nF capacitor passive filter, easily out performs the active filter. The active filter configuration appears to converge to a single value and are indistinguishable at about 65MHz. To overcome this limitation it may be wise to consider adding passive filter elements for frequencies above 20MHz. Adding additional passive filter elements does not uncut the advantages of using an active filter. The active filter still provides additional filtering at frequencies below 20MHz and greatly reduces currently flowing on the chassis.

3.4.3. Time Domain

The final measurements of the proposed active VSCA common mode filter are time domain measurements of the filter output. For these measurements the same setup was used as for the frequency domain measurements. 1MHz 3V peak to peak square wave was applied to the circuit as a noise source. Refer to Figure 3.23 for a schematic of the setup. Figure 3.26 shows the time domain measurements over multiple periods. Figure 3.27 shows the time domain measurement zoomed in around a rising edge on the input waveform.

Reviewing Figure 3.27 gives an intuitive feel for how the active filter performs. The open feedback follows the output with no filter very closely with only amplitude differences. The short and 100Ω feedback configurations follow each other closely. It can be seen that the active filter still

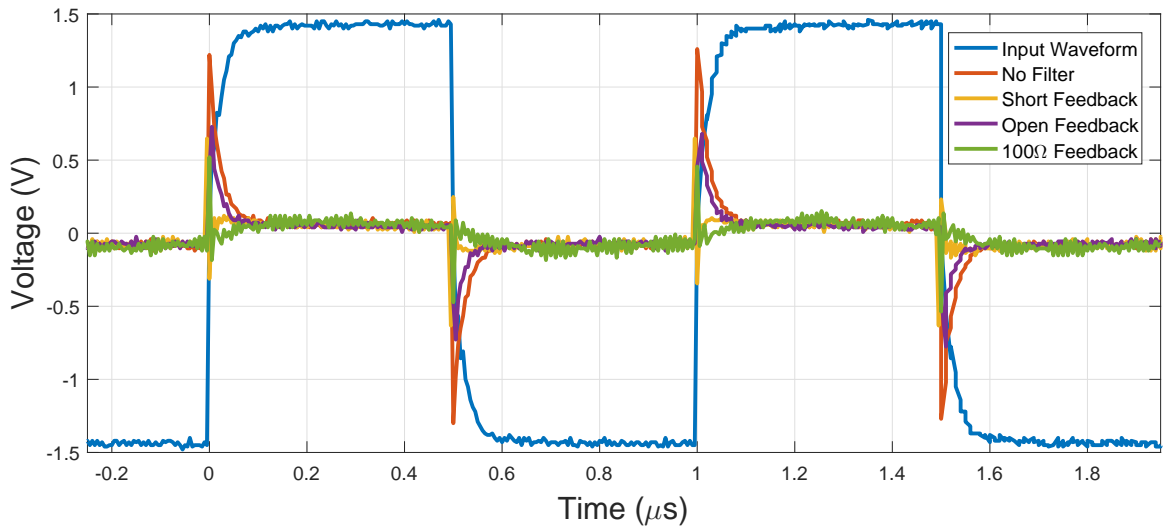


Figure 3.26. Time domain plot of input to the test circuit compared to the output of the test circuit using a shorted feedback configuration, a 100 Ω feedback configuration, and an open feedback configuration. For reference, an output with no filter circuit is also shown.

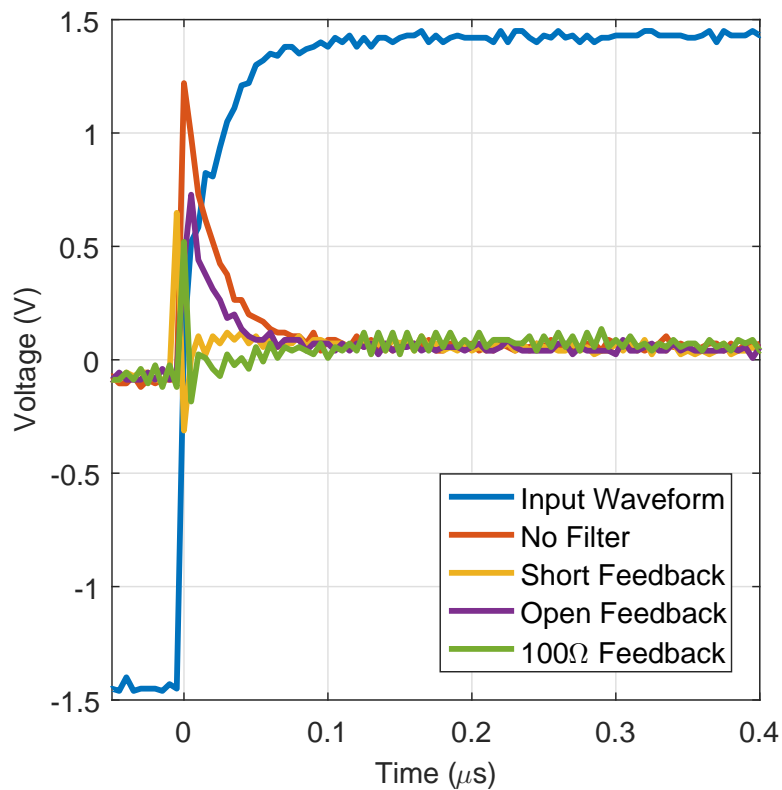


Figure 3.27. Zoomed in time domain plot of filter output with a shorted feedback configuration, a 100 Ω feedback configuration, and an open feedback configuration. For reference, the input waveform and an output with no filter circuit is also shown.

has a lot of high frequency content by the sharp transitions and that some of the low frequency content has been removed by noticing that the decay after the rising edge has been removed.

CHAPTER 4. CONCLUSION

In this thesis, a voltage sensing current adjusting active common mode filter was presented. The proposed filter was designed for DC to DC switched mode power supplies with current draw requirements too large for traditional common mode chokes to be cost effective. The proposed design was analyzed theoretically, simulated, synthesized, and measured. The measured S21 results showed active filtering at 20MHz, much greater than previous designs. The filter also reduces the current measured on chassis connections caused by parasitic capacitance. Measured spectral results with the filter using a 1MHz waveform shows that the active filter outperforms a purely passive filter constructed of similar components over the design frequency range. Several possible filter feedback configurations were analyzed. The study suggests that optimal feedback configurations are not straightforward, but can be tuned in using measurements.

The proposed filter could be used in a variety of applications that cannot use traditional power supply filters. The designed filter can be made to work with power supply system independent of the power supply design current. The filter offers a much smaller and more convenient alternative to common mode choke.

BIBLIOGRAPHY

- [1] L. Roslaniec, A. Jurkov, A. Bastami, and D. Perreault, “Design of single-switch inverters for variable resistance/load modulation operation,” *Power Electronics, IEEE Transactions on*, vol. 30, no. 6, pp. 3200–3214, June 2015.
- [2] H. Ott, *Electromagnetic Compatibility Engineering*. Wiley, 2011. [Online]. Available: <https://books.google.com/books?id=2-4WJKxzzigC>
- [3] C. R. Paul, *Introduction to Electromagnetic Compatibility (Wiley Series in Microwave and Optical Engineering)*. Wiley-Interscience, 2006.
- [4] *CISPR 25: Limits and methods of measurement of radio disturbance characteristics for protection of receivers used on board vehicles*, Comité International Spécial des Perturbations Radioélectriques Std., Rev. 3rd., 2008.
- [5] S. Wang and F. Lee, “Common-mode noise reduction for power factor correction circuit with parasitic capacitance cancellation,” *Electromagnetic Compatibility, IEEE Transactions on*, vol. 49, no. 3, pp. 537–542, Aug 2007.
- [6] G. W. Wester and R. D. Middlebrook, “Low-frequency characterization of switched dc-dc converters,” *IEEE Transactions on Aerospace and Electronic Systems*, vol. AES-9, no. 3, pp. 376–385, May 1973.
- [7] M. H. Nagrial and A. Hellany, “Emi/emc issues in switch mode power supplies (smes),” in *Electromagnetic Compatibility, 1999. EMC York 99. International Conference and Exhibition on (Conf. Publ. No. 464)*, July 1999, pp. 180–185.
- [8] D. M. Pozar, *Microwave Engineering*, 4th ed. Wiley, 2012.
- [9] Fairites. How to choose ferrite components for emi suppression. [Online]. Available: www.fair-rite.com

- [10] L. E. Lawwhite and M. Schlecht, “Active filters for 1-mhz power circuits with strict input/output ripple requirements,” *Power Electronics, IEEE Transactions on*, vol. PE-2, no. 4, pp. 282–290, Oct 1987.
- [11] M. Heldwein, H. Ertl, J. Biela, and J. Kolar, “Implementation of a transformerless common-mode active filter for offline converter systems,” *Industrial Electronics, IEEE Transactions on*, vol. 57, no. 5, pp. 1772–1786, May 2010.
- [12] A. Chow and D. Perreault, “Active emi filters for automotive motor drives,” in *Power Electronics in Transportation, 2002*, Oct 2002, pp. 127–134.
- [13] *Advanced Computer Design*, Ads 2015 ed., Keysight Technologies Inc.
- [14] T. I. Inc. Low noise, high slew rate, unity gain stable voltage feedback amplifier. [Online]. Available: www.ti.com

APPENDIX

The following is a derivation of Equation 3.1 using nodal analysis and Figure 3.1. Assuming an ideal op-amp and using the Kirchhoff's Current Law Equations A.1, A.2, and A.3 can be written.

$$0 = \frac{V_{LISN}(s) - V_{source}(s)}{Z_{source}(s)} + \frac{V_{LISN}(s) - V_A(s)}{Z_{measure}(s)} + \frac{V_{LISN}(s) - V_A(s)}{Z_{measure}(s)} + \frac{V_{LISN}(s) - V_B(s)}{Z_{inject}(s)} + \frac{V_{LISN}(s) - V_B(s)}{Z_{inject}(s)} + \frac{V_{LISN}(s)}{Z_{LISN}(s)} \quad (\text{A.1})$$

$$0 = \frac{V_A(s) - V_{LISN}(s)}{Z_{measure}(s)} + \frac{V_A(s) - V_{LISN}(s)}{Z_{measure}(s)} + \frac{V_A(s) - V_B(s)}{Z_{feedback}(s)} \quad (\text{A.2})$$

$$0 = \frac{V_B(s) - V_{LISN}(s)}{Z_{inject}(s)} + \frac{V_B(s) - V_{LISN}(s)}{Z_{inject}(s)} + \frac{V_B(s) - V_A(s)}{Z_{feedback}(s)} \quad (\text{A.3})$$

Using the properties of an ideal op-amp the voltage $V_A(s)$ is equal to zero, this is expressed in Equation A.4.

$$0 = V_A(s) \quad (\text{A.4})$$

Adding similar terms together and by using Equations A.1, A.2, A.3, and A.4 can be simplified into Equations A.5, A.6, and A.7.

$$0 = \frac{V_{LISN}(s) - V_{source}(s)}{Z_{source}(s)} + 2 \cdot \frac{V_{LISN}(s)}{Z_{measure}(s)} + 2 \cdot \frac{V_{LISN}(s) - V_B(s)}{Z_{inject}(s)} + \frac{V_{LISN}(s)}{Z_{LISN}(s)} \quad (\text{A.5})$$

$$0 = 2 \cdot \frac{-V_{LISN}(s)}{Z_{measure}(s)} + \frac{-V_B(s)}{Z_{feedback}(s)} \quad (\text{A.6})$$

$$0 = 2 \cdot \frac{V_B(s) - V_{LISN}(s)}{Z_{inject}(s)} + \frac{V_B(s)}{Z_{feedback}(s)} \quad (\text{A.7})$$

Rewriting Equation A.6 to solve for $V_B(s)$ gives Equation A.8.

$$V_B(s) = Z_{feedback}(s) \cdot 2 \cdot \frac{-V_{LISN}(s)}{Z_{measure}(s)} \quad (\text{A.8})$$

Inserting Equation A.8 into Equation A.5 leads to Equation A.9.

$$0 = \frac{V_{LISN}(s) - V_{source}(s)}{Z_{source}(s)} + 2 \cdot \frac{V_{LISN}(s)}{Z_{measure}(s)} + 2 \cdot \frac{V_{LISN}(s) - Z_{feedback}(s) \cdot 2 \cdot \frac{-V_{LISN}(s)}{Z_{measure}(s)}}{Z_{inject}(s)} + \frac{V_{LISN}(s)}{Z_{LISN}(s)} \quad (\text{A.9})$$

Grouping $V_{LISN}(s)$ from Equation A.9 leads to Equation A.10.

$$\frac{V_{source}(s)}{Z_{source}(s)} = V_{LISN}(s) \cdot \left(\frac{1}{Z_{source}} + \frac{2}{Z_{measure}(s)} + \frac{2}{Z_{inject}(s)} + \frac{4 \cdot Z_{feedback}(s)}{Z_{measure}(s) \cdot Z_{inject}(s)} + \frac{1}{Z_{LISN}(s)} \right) \quad (\text{A.10})$$

Dividing both sides of Equation A.10 by $V_{LISN}(s)$ and multiplying $V_{SOURCE}(s)$ gives Equation A.11.

$$\frac{V_{LISN}(s)}{V_{source}(s)} = \frac{1}{Z_{source}(s)} \cdot \left(\frac{1}{\frac{1}{Z_{source}} + \frac{2}{Z_{measure}(s)} + \frac{2}{Z_{inject}(s)} + \frac{4 \cdot Z_{feedback}(s)}{Z_{measure}(s) \cdot Z_{inject}(s)} + \frac{1}{Z_{LISN}(s)}} \right) \quad (\text{A.11})$$

Inspection shows that Equation A.11 is the same as Equation 3.1.